MSc thesis in Applied Physics

Towards Universality in the Near-Surface Temperature Profile

Iris Verouden

09-03-2023, Delft

TU Delft

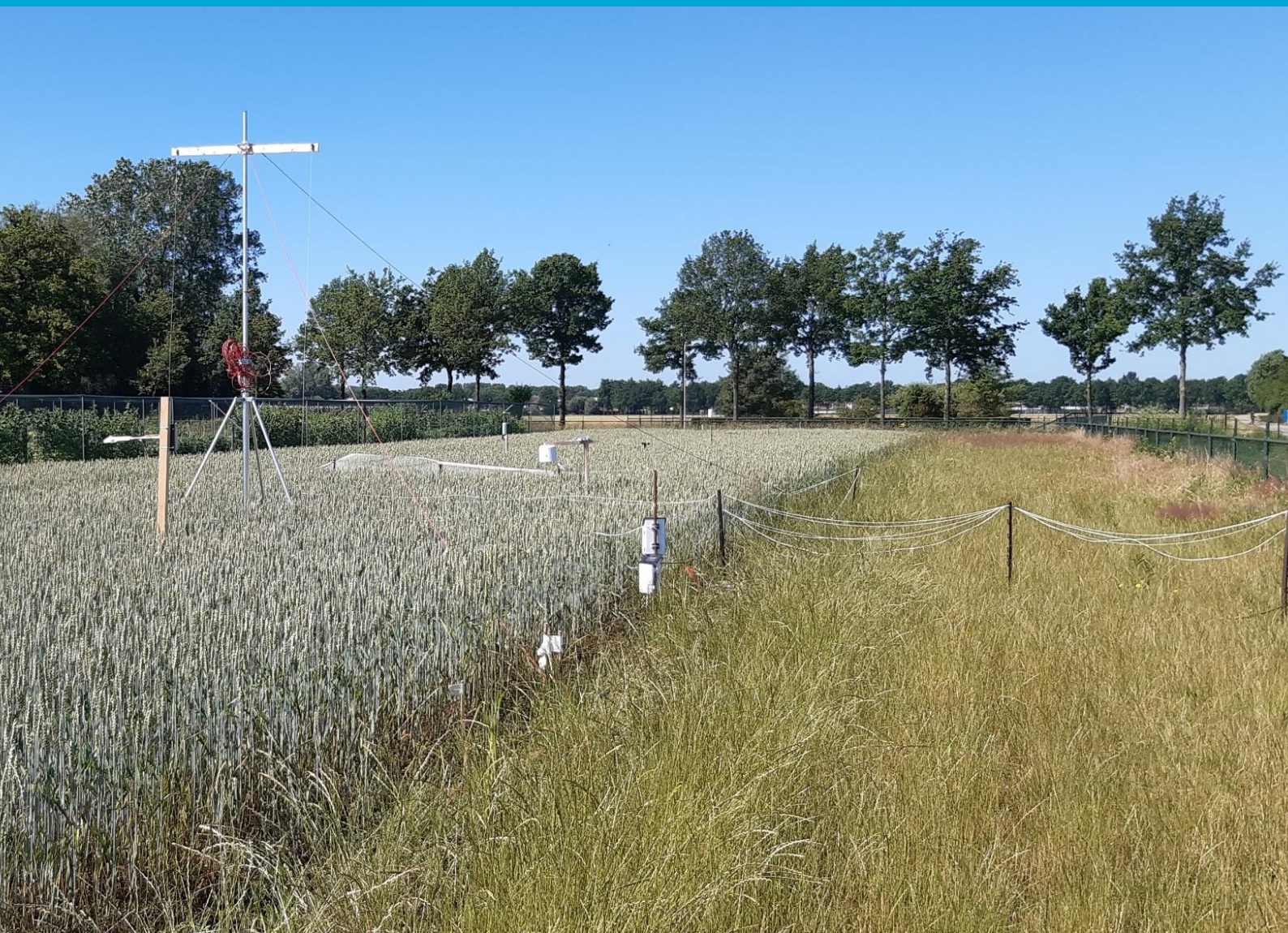

Photo on the cover: Distributed Temperature Sensing measurement set up on the Unifarm of Wageningen University. This is a similar set up as used in this research. Photo taken by Iris Verouden.

MSc thesis in Applied Physics

Towards Universality in the Near-Surface Temperature Profile

Iris Verouden

March 2023

A thesis submitted to the Delft University of Technology in partial fulfillment of the requirements for the degree of Master of Science in Applied Physics

Iris Verouden: *Towards Universality in the Near-Surface Temperature Profile* (2023)

The work in this thesis was carried out in the:

Fruit Frost Group
Clouds and Climate
for Applied Physics
at Applied Sciences
Delft University of Technology

Supervisors:	Prof.dr.ir. Bas van de Wiel
	MSc. Yi Dai
	MSc. Judith Boekee
External supervisors:	Dr. Ir. Marie-Claie ten Veldhuis
	Dr. Ir. Eric Verschuur

Abstract

Weather and climate models require knowledge about the surface temperature and surface heat flux to make predictions for climatology, farming, wind power prediction, etc. Most current models make use of Monin-Obukhov Similarity Theory (MOST). This theory expresses multiple turbulent fluxes in terms of their mean gradients with height. MOST results in an accurate universal form for the non-dimensional wind, temperature and humidity profiles from just above the surface and up to the top of the Atmospheric Surface Layer. The description of the near-surface temperature profile above a rough surface is, however, non-robust and ill-defined in the lowest layer of the atmosphere, the Roughness Sublayer. This thesis presents a new flux-gradient framework based on surface geometry. We apply it to the near-surface temperature profile of high-resolution experimental data from fibre optic measurements over a grass surface. The framework was developed to universally compare 3 different types of models at the surface: a Direct Numerical Simulation in a smooth pipe validated model; a constant surface gradient over grass model and a tall canopy model. Where the temperature is scaled with the already in use turbulent heat flux scale, the new length scale scales the height based on a finite surface gradient which is observed in experimental data. The experimental data can in this framework collapse onto one universal profile with the use of a reference temperature taken at the top of the grass. The framework thus extends MOST with a universal non-dimensional temperature profile in the roughness sublayer.

Acknowledgements

The completion of this thesis would not have been possible without some important people to whom I would like to extend my gratitude.

First of all, I am grateful for my supervisor, Bas van de Wiel. Your energy and extensive experience in the field led to interesting, motivating and helpful meetings. Thank you for your guidance and your time in our many and appreciated meetings during my project.

Next, I would like to thank Judith Boekee and Yi Dai, for your time to answer any small questions I had and the relaxed conversations that we shared over tea. You helped elevate my thesis process as well as product. Furthermore, many thanks to Marie-Claire ten Veldhuis and Eric Verschuur for being part of my thesis committee and taking your time for my graduation.

This thesis project would still not have been possible without some other people. Thanks to my parents, for their patient, loving and motivating words that supported me throughout the project. Special thanks to Roos van Hoften, for being my study buddy and spending many days and weeks on campus to motivate me to work and for being there as a sparring partner for the more supporting topics. Thank you to all my other friends who listened to, sparred and laughed with me throughout this period.

Iris Verouden
March 8, 2023
Delft

Contents

Acronyms

List of Figures

List of Tables

1. Introduction

Weather and climate models require knowledge about the near surface temperature profile to make accurate predictions for climatology, farming and many more applications. There is however no consensus on a universal model for the near surface temperature [1]. There exist different models for the description of the temperature very close to the surface. Unfortunately, the model parameters are often non-robust with high variability in optimal values for their applications. Each model so far has a very specific use case and has been fit to this case, so that a universal model is still lacking.

Most models use the Monin-Obuhkov Similarity Theory (MOST) that has been developed to universally describe multiple transport processes near the Atmospheric Surface Layer (ASL), which is the lowest 10% of the Atmospheric Boundary Layer (ABL) [2]. The ABL is defined as the atmospheric layer that is influenced by the Earth's surface, specifically by surface friction, evaporation, diurnal cycle, etc. MOST results in a basic form of the non-dimensional wind, temperature and humidity profiles. From a few decimetres above the surface upward it is indeed very successful in expressing turbulent fluxes in terms of the mean gradients.

The theory is, however, not defined at the lowest levels of the ASL, which in literature is often called the Roughness Sublayer (RSL). It defines and uses roughness lengths as parameters to characterise the near surface profiles down to the surface. Both the RSL and these roughness lengths have varying definitions. This is in the case of heat and temperature especially non-robust: definitions of the heat roughness length vary between studies and values on same-site measurements can have differences of 3 to 6 orders of magnitude [3, 4].

This non-robustness is exactly what this thesis will focus on: the research goal is to find a robust and universal parameter specifically for the near surface temperature profile. The focus will be from the surface up, as this is where MOST mostly deviates from measurements. The atmosphere interacts with the surface below depending on the surface geometry and the vegetation that is part of that geometry. A measure of this geometry would then be an important parameter to find for characterisation of the near surface temperature profile.

This research will take two main steps: developing a flux-gradient framework for heat exchange based on surface geometry and using experimental data to analyse different models in the framework. This work builds on the thesis from Nollen (2022) [5]. This thesis includes a short review of his findings and what that would mean for our research goal. Using this knowledge, a new, non-dimensional framework is then developed with use of models from Nollen and models found in literature, for a total of 3 different types of models. This framework introduces scaling parameters for the temperature and height from the surface, of which the length parameter will be specifically derived from the surface geometry. Afterwards, the framework is applied to experimental Distributed Temperature Sensing (DTS) data that has a high vertical resolution. This data is then used to evaluate the models.

The structure of this thesis is as follows. Chapter 2 describes the status quo of research into the near surface characteristic flow parameters more in-depth. It will also introduce the models which will be analysed during this research. Then, the developed framework is

presented in chapter 3 and applied to the models. Chapter 4 moves towards the experimental step of this thesis and will present the experimental methods of the research, from the DTS set ups, to data selection and the comparison to the models. The results, both from the revision of Nollen's work [5] as well as our own steps, will then be presented in chapter 5. Chapter 6 provides the interpretation and discussion of the results and will follow up with the recommendations for future research. The main conclusions from this thesis can then be found in chapter 7.

2. Theory

This chapter will start with a short introduction to the near-surface atmosphere and the current model to describe the near-surface temperature profile. Current models base their temperature profile description on MOST, which will be explained. This chapter then introduces potential alternatives for the near-surface temperature profile description.

2.1. Background

The Atmospheric Boundary Layer (ABL) is a complex system, where many different physical processes may play a role at the same time. The flow and transport phenomena in the ABL can be described as a specific case of turbulence. The system can be approximated as turbulent flow above a wall. Turbulent descriptions of this specific case exist [6, 7], but research is still active for different and more specific cases of atmospheric flow [8]. The different processes present in the ABL are radiation, turbulent mixing, phase transitions, heat conduction, etc. The focus of this thesis lies on turbulent heat transport.

In atmospheric science, the ABL is a very important concept to understand. The ABL is defined as a layer closest to the surface which is capped off by an inversion layer, above which the characteristics of the atmosphere significantly change. The characteristics of the ABL constantly change in a diurnal cycle, as the processes previously described can depend on the Sun. The surface has significant influence on the characteristics of the flow in the ABL and most of the mixing happens here as well [2].

In turbulent descriptions flow above a wall is characterised by the law of the wall. This law distinguishes separate regimes: bulk flow, where the flow is mostly driven by large scale pressure differences; the log layer, where the wall starts to influence the bulk flow and shear driven turbulence becomes more important; down to the viscous layer, where the flow is characterised by the smallest scales and the fluid viscosity [6, 7]. The different regimes have different flow descriptions and behave differently. Models try to accurately describe the flow over these regimes, along with the transitions between the different regimes.

Expanding this knowledge to the atmosphere proves to be a challenge. Models show high variability in surface temperature especially over land and ice depending on the flow parametrisations used [1]. Figure 2.1 shows the average difference between two versions of the European Centre for Medium-Range Weather Forecasts (ECMWF) model where the impact of stability is analysed. This study was first done in 1999 and repeated with newer models in 2010. Both studies show large differences between the two stability parametrisations for the 2m temperature over land and ice, with an increase in the differences in the newer version of the ECMWF model. Important to note is the high spatial variability, meaning that the models try to take the specific surface into account. This means that it is still a unclear how to exactly model or parametrise the surface temperature.

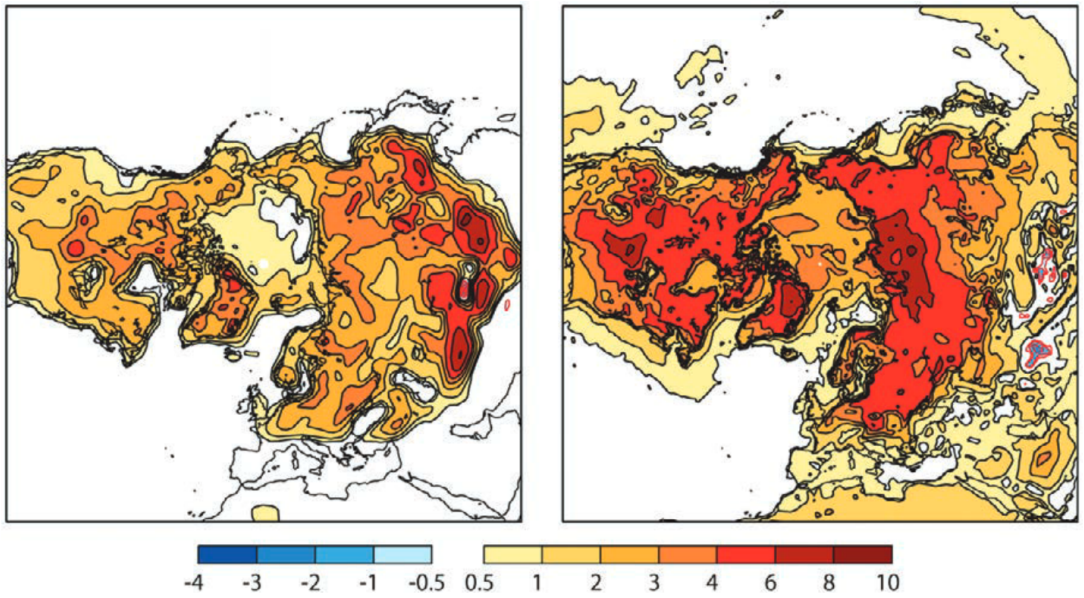

Figure 2.1.: Temperature difference at 2m [°C] between 2 versions of models with differing stability description, study done in 1999 (left) and 2010 (right). The analysed period was January of 1996 and the difference between the 2 models are averaged [1].

Figure 2.2 shows definitions of the commonly identified layers in the lowest layer of the ABL. The atmospheric surface layer (ASL) is defined as the lowest layer of the ABL where the turbulent flux values throughout this layer do not change more 10% from each other. Thus, by definition the ASL has rather uniform values for the turbulent fluxes throughout the layer.

Within this surface layer the canopy stands at a height of h_c, this indicates the edge of the canopy layer. The canopy adds friction for the air flow through and above the canopy. The friction is plays a role in the transport of for example heat in the Roughness Sublayer (RSL), which height is denoted by z^*. This layer starts above the canopy, as the flow of the atmosphere gets obstructed by the roughness elements and pushed up above the canopy. This generates strong turbulence in this layer, which is not as strongly present in the ASL.

The roughness sublayer height z^* has different definitions, not just the $1.6h_c$ from the figure. It can depend on the canopy height h_c as in figure 2.2, but models also make use of the so called displacement height d, the roughness height z_0, the average horizontal inter-element spacing δ, or a combination of these parameters [9].

The displacement height d in particular is used to displace the zero plane to the apparent surface of the atmosphere. The interpretation of d is either the height at which the canopy exerts drag on the flow through it, or the displacement height which is used in fluid mechanics [2]. For example in a maize field, the wind would be able to penetrate the top layer, but it would stop at a certain height in between the stalks. This height would then be considered the zero-plane for the transport phenomena. The value of the displacement height can be taken as $d = 2/3h_c$ but also has different definitions. Because there are such varying parametrisations, it is important to understand the precise definitions of the parameters in the investigated model, whether that be d, z^* or other.

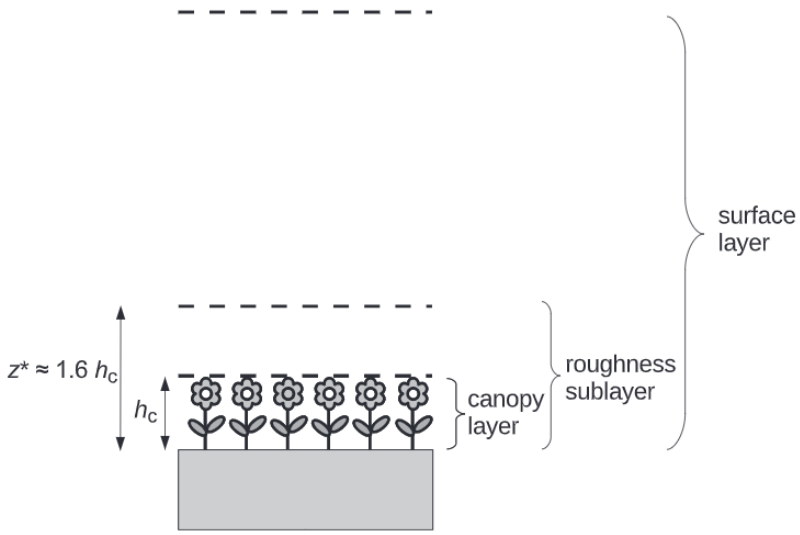

Figure 2.2.: A schematic illustration of the different atmospheric layers found near the surface [2].

2.2. Status quo

The traditional description of the transport processes in the atmosphere are defined in the ASL, but not the RSL. The large scale turbulent eddies at the top of the ASL, break down into smaller scale eddies closer to the surface. The break up of eddies is driven by inertia as energy is conserved. Because the eddies decrease in size towards the surface, a larger wind speed gradient is required for the vertical transport of heat and momentum. This is the principle of the law of the wall and results in a characteristic logarithmic behaviour of the wind speed and temperature profiles.

This logarithmic behaviour is captured in Monin-Obuhkov Similarity Theory (MOST). This theory was empirically designed for the description of turbulent characteristic quantities in the ABL, but above the RSL [2]. It connects vertical gradients to surface fluxes of different quantities, such as wind speed, temperature, moisture, etc. MOST tries to compose a universal and similar function for turbulent properties in the lower part of the atmosphere, given the characteristic properties of the surface and the flow above it. This means that the theory developed one formulaic form for momentum, heat or other transport. For MOST to have this similarity, restrictions apply:

- Stationarity, the mean of the described property should not depend on time
- Horizontal homogeneity, the mean of the describe property should not depend on the horizontal placement
- The turbulent properties should only depend on the surface processes.

Once those conditions are met, MOST can connect the vertical turbulent fluxes to the vertical gradients of the mean profiles of the desired turbulent characteristic. The MOST gradient

functions for mean wind velocity $U[m/s]$ and mean potential temperature θ [K] can be universally written in non-dimensional form as [2]

$$\frac{\partial U}{\partial z}\frac{\kappa z}{u_*} = \phi_m \qquad \text{and} \tag{2.1a}$$

$$\frac{\partial \theta}{\partial z}\frac{\kappa z}{\theta_*} = \phi_h, \qquad \text{(MOST)} \tag{2.1b}$$

where ϕ_i, for $i = m, h$ is the dimensionless universality function for momentum and heat respectively, u_* turbulent velocity scale [m/s], θ_* [K] the turbulent temperature scale and κ the Von Kármán constant. The height z here is taken as the height above the surface. These functions ϕ, also called the flux-gradient relationships or the similarity functions, depend on the investigated quantity as well as stability of the atmosphere.

In meteorology, atmospheric stability plays an important role in weather and atmosphere characteristics. Stability is the ratio between buoyancy and shear that either produce or dissolve turbulence in the atmosphere. An unstable atmosphere means that there is much turbulence, due to warm air below cold air where buoyancy generates vertical motion or by large shear of the wind flowing over the surface. In the stable case, warm air above cold air suppresses turbulence and dampens the mixing effect in the atmosphere [2]. In the very stable case, stratification will occur. This means that little mixing will result in horizontal layers that have somewhat uniform values for turbulent transport.

In turbulent models the Von Kármán constant is an important factor to align the models with experiments. In experimental set ups and most flows, the constant $\kappa = 0.40 \pm 0.02$ is common to use. While for atmospheric cases the Von Kármán constant can vary over a wider range, it is also accepted to use $\kappa = 0.40$ and models often use this value to align with experimental data [10].

The characteristic turbulent scales u_* and θ_* are a measure of the turbulent fluctuations of their respective mean property. In the case of the velocity fluctuations, this is called the friction velocity. Friction velocity means that the friction in the air induces fluctuations to the wind speed. These turbulent scales are used to connect to the fluxes of momentum and heat respectively to their gradients. For example $\theta_* = -H/\bar{\rho}c_p u_*$, with H the surface sensible heat flux. These scales have been designed in this way to describe the MOST relations in a non-dimensional manner.

An important parameter in MOST is the Obukhov length L, defined as

$$L = \frac{\bar{\theta_v} u_*^2}{\kappa g \theta_{v*}}, \tag{2.2}$$

where $\bar{\theta_V}$ is the mean absolute virtual temperature [K] and g the gravitational acceleration constant $[m/s^2]$. The dimensionless parameter z/L can be linked to atmospheric stability. In case $z/L > 0$ turbulence is suppressed by buoyancy and the atmosphere is stable. Vice versa, $z/L < 0$ indicates an unstable atmosphere.

The similarity functions ϕ are a function of z/L, and are different per stability cases. The universality functions have been heavily researched and have different possible forms. They can be described via the Businger-Dyer flux-gradient relationships: [2]

$$\phi_i = \left(1 + \alpha \frac{z}{L}\right)^n, \tag{2.3}$$

thus with α and n coefficients dependent on stability and the turbulent variable described. Following the Businger-Dyer relationships, the stable case is described by $\alpha = 5$ and $n = 1$ for both momentum and heat. This is in the unstable case $\alpha = -16$ and $n = -1/4$ for momemtum and $n = -1/2$ for heat. Important to note is that for $z << L$, the dependency on the Obukhov length disappears and the stability function ϕ_i becomes equal to 1. This is similar to a neutral case where stability can be ignored.

In many practical applications, the near-surface turbulent characteristic values are useful to describe the vertical differences. However, MOST is undefined in this area as using $z = 0$ in the logarithmic profiles is undefined. Another definition for the surface height is required for the model. In the case of momentum it is clear that this height is where the no-slip condition should be applied, the height at which the wind speed becomes zero due to the roughness of the surface. For temperature this assumption is not as clear. Traditionally, the surface temperature is measured, for example by measuring the emitted longwave radiation, and the profile is extrapolated down to the height of this temperature. The height of this determined surface temperature is then determined as the roughness height for heat.

The roughness height z_{0i}, for $i = m, h$ for momentum and heat respectively, is illustrated in figure 2.3. The figure also shows that from a certain point the logarithmic regime (full line) is extrapolated towards the expected values for the wind speed and temperature at their respective roughness heights. Unlike momentum, heat is not dissipated by drag but by molecular diffusion, which is less effective for transport. This means that the value of z_{0h} is lower than that of z_{0m}. The roughness height for heat z_{0h} is often taken as $z_{0h} = 0.1 z_{0m}$ or the ratio z_{0m}/z_{0h} is investigated.

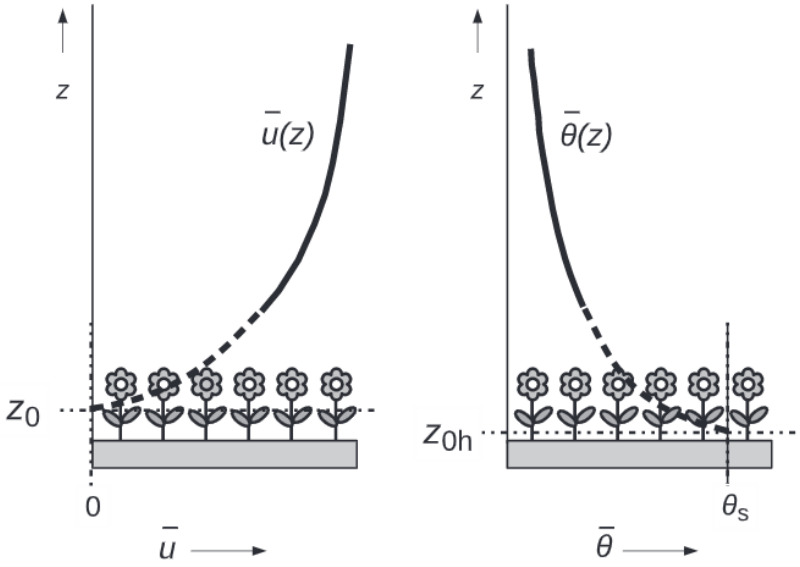

Figure 2.3.: Definitions of the roughness heights for momentum z_{0m} (left, z_0 in this figure) and heat z_{0h} (right) along with their mean property profile in the case where surface roughness is caused by vegetation. The full lines are the logarithmic regime in the ASL and the dashed lines indicate the approximated profile in the RSL following the extrapolated logarithmic profile down to the roughness heights [2].

For MOST the roughness height is used as an integration constant for the definition of the profiles. If stability is ignored (neutral or $z << L$ case) this results in

$$U(z) = \frac{u_*}{\kappa} \ln\left(\frac{z}{z_{0m}}\right) \qquad \text{and} \tag{2.4a}$$

$$T(z) - T_s = \frac{\theta_*}{\kappa} \ln\left(\frac{z}{z_{0h}}\right), \tag{2.4b}$$

where T_s is considered the surface temperature at z_{0h}. In this thesis we are considering the absolute air temperatures, thus we use T. Very close to the surface, this is close to the potential temperature described before.

The value for the roughness length for heat for a single site can range between 3 to 6 orders of magnitude [3, 4]. This would result in an uncertain predicted surface temperature and surface heat flux. Figure 2.4 shows that the roughness height for heat is not accurately defined. Some models use that the ratio $z_{0h}/z_{0m} \approx 0.1$, but different values of this ratio are also found in literature and measurements as indicated in figure 2.4a [3]. This figure shows that the spread for this ratio on 1 site can range 6 orders of magnitude. Figure 2.4b shows the performance of predicting θ_* for different calculated z_{0h}. $\theta_{*,calc}$ is calculated using different values for z_{0h} and is compared against the measured $\theta_{*,ec}$ using the eddy covariance method. The different values for z_{0h} were based on different studies for the same measurement site, yet show a large difference in performance.

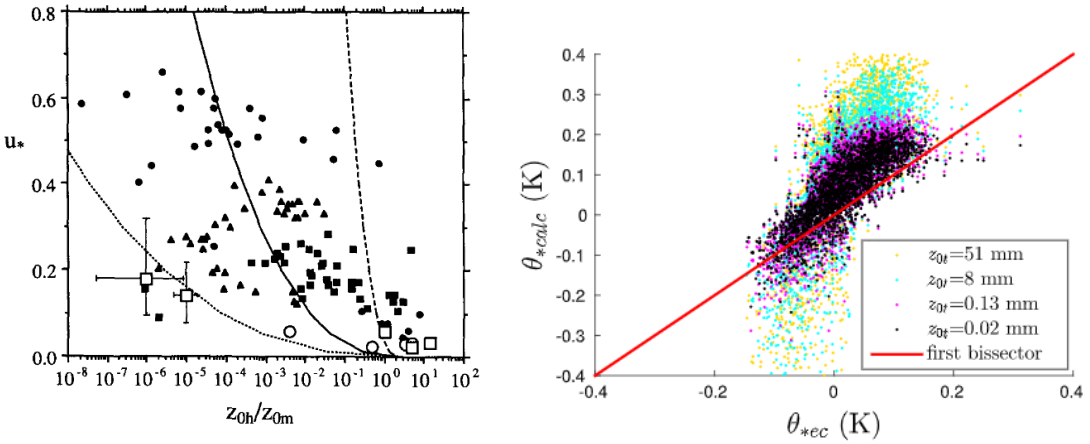

(a) (b)

Figure 2.4.: The left figure (a) shows results of experiments in Cabauw, the Netherlands, to determine the ratio of roughness lengths with spread varying over 6 orders of magnitude [3]. On the right (b) a study on the Antarctic tundra is the calculated (subscript calc) versus measured (subscript ec for eddy covariance) turbulent heat scale that shows a spread for different roughness heights $z_{0h} = z_{0t}$ denoted by the different colours in the legend [4].

Per measurement site z_{0h} should be deduced once and that value will then be used in the later modelling for the surface temperature. However, the large spread in z_{0h} values for a single site suggests that its underlying concept has a limited universal character. That is: with a solid physical concept the parameters should be well-defined (robust) for a single site. The fact that this is not the case suggests that the concept/model can be improved.

2.3. Other models

As the current model is non-robust, research delves into newer models as alternatives for their specific use cases [8]. For this thesis, 3 different models have been identified that could describe flow above a vegetated surface. These are the *z plus b model* [5], the *van Driest model* [11, 12] and the *de Ridder model* [9]. These models build on MOST for the surface layer, but aim to refine and improve the profile descriptions in the layers below in order to achieve a higher degree of realism. This section will introduce and explain each model in order.

The z plus b model was developed by Paul Nollen [5] during his thesis as an empirical approximation to his measurement data. The experiment was conducted over grass using a high resolution DTS set up ranging from 10m down to the surface. In the traditional temperature profile description, the length scales become zero close to the surface. This would mean that the gradient at the surface is infinite. Nollen [5] found that that the temperature profile reaches a finite gradient near the surface. He then proposes a finite length scale b [m] to reflect this behaviour in the near-surface temperature profile and gradient description.

Adding this length scale to arrive at a finite surface gradient into Eq. 2.1b results in

$$\frac{\partial \theta}{\partial z} = \frac{\theta_*}{\kappa(z+b)}\phi_h, \tag{2.5}$$

where z in Eq. 2.1b is replaced by $z+b$ and b is thus a separate length scale parameter like the roughness height z_{0h}. Nollen's main goal was to arrive at a parameter that could be dependent on the surface geometry, in this case the grass height. In his research he reached the conclusion that b is of the order of half the grass height to best align with his case.

The Van Driest model was used by Donda et al. [11, 12], who built on the description of flow near a wall as described by Van Driest and added viscosity in their equation. The paper discusses this in the context of smooth channel flow in the stably stratified case. This is then investigated using a Direct Numerical Simulation (DNS) model, which in similarity analysis provides an adequate approximation of atmospheric processes. They find that their addition of the viscous forces in the model leads to a close approximation of the DNS profiles even in the near-surface range.

In Donda's papers, they add the influence of viscosity to turbulent flow. The bulk and log layer are well defined until the flow is nearing the wall. Closer to the wall, the turbulent scale will become smaller and will in the end thus be dependent on viscosity. The paper arrives at a definition for the friction velocity as [11, 12]

$$u_*^2 = \left[\frac{(A\kappa z)^2}{(1+\alpha\frac{z}{L})^2}\frac{\partial U}{\partial z} + \nu\right]\frac{\partial U}{\partial z}, \tag{2.6}$$

where $A = 1 - \exp(-\beta \mathrm{Re}_*)$ [-] is the so-called Van Driest function and ν [m^2/s] is the kinematic viscosity. The Van Driest function pinches the logarithmic model and thus decreases the vertical turbulent transport as z becomes small, giving the fluid viscosity more significance. In the Van Driest function β [-] is an empirical constant and Re_* is the friction Reynolds number which depends on the surface friction velocity, channel depth and fluid viscosity. When using this model, these parameters need to be determined beforehand. In the case above grass, the channel depth is not defined and another height scale should be used. Important to note is that a MOST stability function $(1 + \alpha z/L)$ can be identified.

This research focuses on the turbulent heat flux scale and the model for heat transfer. By combining eqs. 2.1a and 2.1b we can convert the expression for momentum into the following expression for heat:

$$\kappa z = \frac{u_*}{\partial U/\partial z} = \frac{\theta_*}{\partial \theta/\partial z}. \tag{2.7}$$

Using this in Eq. 2.6 results in an expression for the turbulent heat flux scale

$$\theta_* = \left[\frac{(A\kappa z)^2}{\theta_*(1+\alpha\frac{z}{L})^2}\frac{\partial\theta}{\partial z} + \frac{\nu}{u_*}\right]\frac{\partial\theta}{\partial z}. \tag{2.8}$$

The De Ridder model is in principle a tall canopy model [9]. It strives to extend MOST to account for the roughness sublayer (RSL) effects on the flow characteristics. They verify this approach against experimental flux data over a boreal forest in Canada. As these types of forests are often tall, of the order of 14m, they argue that the RSL elongates and its effects become more prominent in the ASL. They extend MOST with a new function which is dependent on the roughness height z^* (z_* in their paper), or in non-dimensional form z/z^*. For this model, the $z = Z - d$ definition is specifically used, meaning that they use the height from the displaced zero-plane.

Including the RSL influence in MOST gives [9]

$$\frac{\partial U}{\partial z}\frac{\kappa z}{u_*} \cong \Phi_M(z/L)\phi_M(z/z^*) \qquad \text{and} \tag{2.9a}$$

$$\frac{\partial \theta}{\partial z}\frac{\kappa z}{\theta_*} \cong \Phi_H(z/L)\phi_H(z/z^*), \tag{2.9b}$$

where in this case the captial Φ_i are the MOST universality or stability functions seen before and the lower case ϕ_i are the new non-dimensional functions describing the RSL effects. There are different descriptions of these RSL functions, De Ridder uses

$$\phi_i(z/z^*) \approx 1 - e^{-\mu_i z/z^*}, \tag{2.10}$$

where μ_i is an empirical coefficient. This form of ϕ was mainly preferred during de Ridder's research as it was a continuous description which form could be used both for the momentum and heat descriptions. Where Donda et al. [11, 12] add the viscous forces, de Ridder [9] introduces the roughness height z^*. They both introduce a sort of pinching function, which is an indication of the height at which their respective forces stop working as z increases. Important for the use of this model is then the experimental determination of the μ coefficient and the RSL height z^* as a first step in using this model.

In short, each model has their own method of including the effects of the surface in the base Monin-Obukhov Similarity Theory. The z plus b model includes an empirically motivated constant surface gradient. The Van Driest model builds upon the smooth channel flow in turbulence models and adds in the viscous effects near the wall, which has been validated using DNS simulations. Finally, the De Ridder model includes the RSL effects in the model and validated this experimentally in a tall canopy.

An overview of the important functions for this thesis is included below.In these forms, the influence of stability is left out as very close to the surface, its influence should become very close to 1. This research specifically investigates the profiles in the RSL, which is below the Obukhov length. We can see this in the universality functions of the from $(1 + \alpha z/L)^n$,

which as $z << L$ becomes 1. Due to the complexity of the van Driest function with the squared temperature gradient after resolving the brackets, this is left in a different form than the other functions. In chapter 3, we will continue with these functions.

$$\text{(MOST)} \qquad \frac{\partial T}{\partial z} = \frac{\theta_*}{\kappa z}$$

$$\text{(z + b model)} \qquad \frac{\partial T}{\partial z} = \frac{\theta_*}{\kappa (z + b)}$$

$$\text{(Van Driest)} \qquad \theta_* = \left(\frac{(A\kappa z)^2}{\theta_*} \frac{\partial T}{\partial z} + \frac{\nu}{u_*} \right) \frac{\partial T}{\partial z}$$

$$\text{(De Ridder)} \qquad \frac{\partial T}{\partial z} = \frac{\theta_*}{\kappa z} \left(1 - e^{-\mu z / z^*} \right)$$

3. Theoretical framework

Chapter 2 introduced the models that will be investigated in this thesis, while this chapter will detail the new flux-gradient framework that helps comparing these models. This requires a non-dimensional form with characteristic scales for the different variables. This makes it possible to compare for example lab data with experimental or outdoor data. This means that we need to find characteristic scales for the temperature and height and develop a method to scale the models. This chapter will detail the scaling steps per model and provide an overview of the resulting scaled functions. An important note is that we neglect stability in this research, as the area of interest means $z << L$ and the stability component will then become equal to 1.

In MOST, the temperature is non-dimensionalised using the turbulent heat flux scale θ_*. This scaling parameter still works close to the surface and will be used in this framework as well.

The other characteristic scale used traditionally for the height is the Obukhov length L in the from of z/L. This L leads to problems very close to the surface, as the z/L term begins to vanish. In the logarithmic description of the temperature profile, the gradient near the surface becomes infinite as z becomes smaller. The roughness height z_{0h} was introduced as a cut-off point for these infinite gradients, but this is, as discussed, non-robust. In reality, the near-surface temperature gradients are finite. By using this finite gradient for the second scaling parameter, we can then write a non-dimensional form for each model.

A consequence of using the surface gradient as a scaling parameter is that all surface gradients become 1 at the surface. We can use this as a practical first step in our framework as taking the limit of $z \to 0$. We can then rewrite the different models with the scaling parameters to arrive at a simple formula for the gradient.

At the end, the slope of the scaled gradient in the limit of $z \to 0$ is shortly investigated. The second derivative could provide insight in the differences between each model.

3.1. The z plus b model

Starting with the first step of taking the limit of $z \to 0$ for equation Eq. 2.5:

$$\begin{aligned} \lim_{z\to 0} \frac{\partial T}{\partial z} &= \lim_{z\to 0} \frac{\theta_*}{\kappa(z+b)}, \\ \left.\frac{\partial T}{\partial z}\right|_{z=0} &= \frac{\theta_*}{\kappa b}. \end{aligned} \tag{3.1}$$

This gives the opportunity to derive the scaled temperature $\hat{T} = T/\theta_*$, this is already the non-dimensionalisation present in classic MOST as indicated. The κb term is then the length

scale present to scale the height in the equation. Interestingly, Eq. 3.1 can be rewritten as

$$\frac{\theta_*}{\partial T/\partial z|_{z=0}} = \kappa b = \mathcal{L}_b, \tag{3.2}$$

where $\mathcal{L}_b$ is the identified length scale for the z plus b model. Here we see different definitions for the length scale, where the surface gradient $\partial T/\partial z|_{z=0}$ is the finite surface gradient we expected at the start of this chapter. The b variable is in Nollen's research related to the grass height [5], which would be another parameter dependent on surface geometry. The relation between the two definitions for the length scale $\mathcal{L}_b$, will be interesting to use during further analysis of experimental data. Finally $\hat{z} = z/\kappa b = z/\mathcal{L}_b$.

Provided these scaling parameters, the non-dimensional version of Eq. 2.5 then becomes:

$$\frac{\partial \hat{T}}{\partial \hat{z}} = \frac{1}{\kappa \hat{z} + 1}. \tag{3.3}$$

In the limit of $\hat{z} \to 0$, this equation becomes 1 and our scaling has worked as intended. To further analyse the behaviour of the profiles, the second derivative

$$\frac{\partial^2 \hat{T}}{\partial \hat{z}^2} = -\frac{\kappa}{(\kappa \hat{z} + 1)^2}, \tag{3.4}$$

is considered in the limit of $\hat{z} \to 0$:

$$\left.\frac{\partial^2 \hat{T}}{\partial \hat{z}^2}\right|_{\hat{z}=0} = -\kappa. \tag{3.5}$$

3.2. The Van Driest model

In the van Driest model case, taking the first step in the scaling process is possible with the current equation as given in the overview in chapter 2. By taking the limit of $z \to 0$ it becomes

$$\begin{aligned} \lim_{z\to 0} \theta_* &= \lim_{z\to 0} \left(\frac{(A\kappa z)^2}{\theta_*} \frac{\partial T}{\partial z} + \frac{\nu}{u_*} \right) \frac{\partial T}{\partial z}, \\ \theta_* &= \left(0 \cdot \frac{\partial T}{\partial z} + \frac{\nu}{u_*} \right) \left.\frac{\partial T}{\partial z}\right|_{z=0} \\ \left.\frac{\partial T}{\partial z}\right|_{z=0} &= \frac{\theta_* u_*}{\nu}. \end{aligned} \tag{3.6}$$

In a similar way as in the first section, it follows that $\hat{T} = T/\theta_*$. Here it is important to note that ν/u_* has the dimension of length, $[m^2 s^{-1}/m s^{-1}] = [m]$, and it would thus be the scaling parameter for this model: the so-called viscous length scale. This is written as $\hat{z} = z u_*/\nu = z/\mathcal{L}_d$, with $\mathcal{L}_d$ the length scale for the Van Driest model.

We apply these scaling parameters to the original model of Eq. 2.8 by substituting $\mathcal{L}_d\hat{z}$ for every z, rewriting the equation and then using the expression for $\hat{T}$:

$$\begin{aligned} 1 &= \left(\frac{(A\kappa\mathcal{L}_d\hat{z})^2}{\theta_*\mathcal{L}_d} \frac{\partial T}{\partial \hat{z}} + \mathcal{L}_d \right) \frac{\partial T}{\theta_*\mathcal{L}_d \partial \hat{z}}, \\ 1 &= \left((A\kappa\hat{z})^2 \frac{\partial \hat{T}}{\partial \hat{z}} + 1 \right) \frac{\partial \hat{T}}{\partial \hat{z}}. \end{aligned} \tag{3.7}$$

This still needs some rewriting to arrive at the equation for the scaled temperature gradient. By resolving the brackets and using the quadratic formula, we arrive at

$$\frac{\partial \hat{T}}{\partial \hat{z}} = \frac{-1 + \sqrt{1 + 4(A\kappa\hat{z})^2}}{2(A\kappa\hat{z})^2}. \tag{3.8}$$

For this research, we determined by analysing the limit behaviour for this model that $A = 1 - \exp(-\beta\hat{z})$ with $\beta = 0.9$.

For the analysis of its second derivative near $\hat{z} = 0$, we rely on the square root case of the binomial series $(1+x)^{1/2} = 1 + \frac{1}{2}x - \frac{1}{8}x^2 + \frac{1}{16}x^3 - \dots$. Eq. 3.8 then becomes

$$\frac{\partial^2 \hat{T}}{\partial \hat{z}^2} = \frac{-1 + 1 + 2(A\kappa\hat{z})^2 - (A\kappa\hat{z})^4 + \dots}{2(A\kappa\hat{z})^2} = 1 - (A\kappa\hat{z})^2 + \dots \quad . \tag{3.9}$$

In the case of $\hat{z} = 0$ the derivative of the gradient then becomes 1.

3.3. The De Ridder model

Before starting with the first scaling step for this model, we expand the exponent for simplicity using the Taylor series $e = \sum_{k=0}^{\infty} z^k/k!$. This will help in taking the limit of the equation in a way that can help determine the scaling parameters. As we are interested in the near-surface temperature gradient, we can leave out higher order terms. These terms will disappear as z becomes small and will thus not influence the result. Using the Taylor series, we arrive at

$$\frac{\partial T}{\partial z} = \frac{\theta_*\gamma z - \frac{1}{2}\theta_*\gamma^2 z^2}{\kappa z}, \qquad \text{with} \qquad \gamma = \mu_h/z^*. \tag{3.10}$$

We can then proceed to the first step in the scaling process, taking the limit gives

$$\begin{aligned} \lim_{z\to 0} \frac{\partial T}{\partial z} &= \lim_{z\to 0} \frac{\theta_*\gamma - \frac{1}{2}\theta_*\gamma^2 z}{\kappa} \\ \left.\frac{\partial T}{\partial z}\right|_{z=0} &= \frac{\theta_*\gamma}{\kappa}. \end{aligned} \tag{3.11}$$

For $\gamma = 1/b$ which has the units $[m^{-1}]$, this gives similar result as for z plus b model. Similarily to the other models, the scaling parameters will then be $\hat{T} = T/\theta_*$ and $\hat{z} = z\gamma/\kappa = z/\mathcal{L}_r$, with $\mathcal{L}_r$ the length scale for the de Ridder model.

Applying these scaling parameters to Eq. 2.9b and Eq. 2.10 results in

$$\begin{aligned} \frac{\partial \hat{T}}{\partial \hat{z}} &= \frac{1}{\kappa \hat{z}} \left(1 - e^{-\kappa \hat{z}}\right) \qquad \text{or as:} \\ \frac{\partial \hat{T}}{\partial \hat{z}} &= 1 - \frac{1}{2}\kappa \hat{z} + \frac{1}{6}\kappa^2 \hat{z}^2 - \dots \quad . \end{aligned} \tag{3.12}$$

The second derivative becomes

$$\frac{\partial^2 \hat{T}}{\partial \hat{z}^2} = -\frac{1}{2}\kappa + \frac{1}{6}\kappa^2 \hat{z} - \dots \tag{3.13}$$

and in the limit of $\hat{z} \to 0$ becomes

$$\left.\frac{\partial^2 \hat{T}}{\partial \hat{z}^2}\right|_{\hat{z}=0} = -\frac{1}{2}\kappa. \tag{3.14}$$

3.4. Overview

Equations 3.3, 3.8 and 3.12 each provide a scaled model where the gradient starts at 1 for $\hat{z} = 0$. For each model, the scaling parameters were $\hat{T} = T/\theta_*$ and $\hat{z} = z/\mathcal{L}_i$, with $i = b, d, r$. The different surface length scales all can be determined with the gradient at the surface and the turbulent heat flux scales, see Eq. 3.2, and are thus the same for each model $\mathcal{L}_s$. Figure 3.1 shows the scaled gradient models together in a graph.

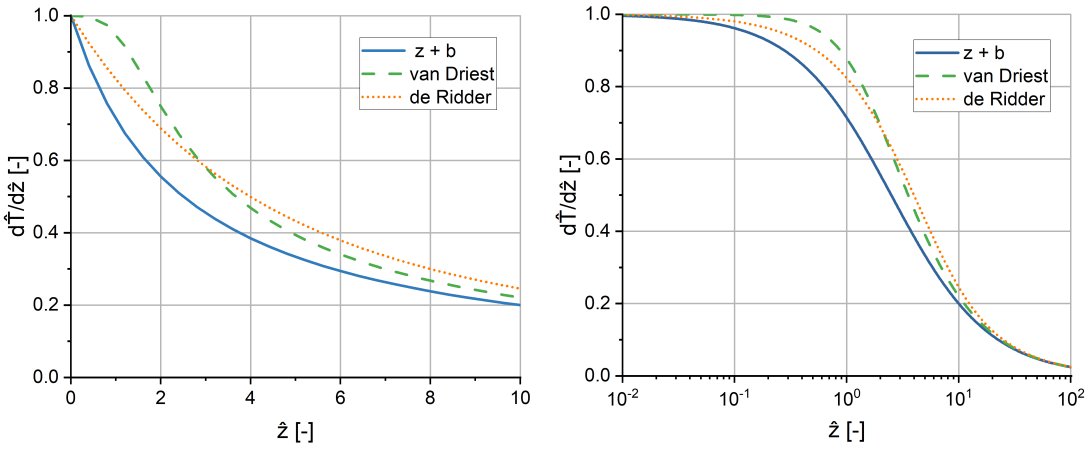

Figure 3.1.: Gradients of the different scaled models on a linear (a) and a logarithmic (b) scale.

The numerically integrated temperature profiles are shown in figure 3.2. Analytical integration of the resulting scaled equations is possible, but for the aim of this research, numerical integration was more convenient. This was executed with the `scipy.integrate.quad` function in python, which is based on a technique from the FORTRAN library. A short note with more details on the integration of the models is included in appendix A. In the upper

regime, the models all increase logarithmically and seem to approach a similar slope. This suggests that the models still follow the MOST model in the upper regime. The offset is due to the different gradients in the lower regimes, which we can see in figure 3.1. Indeed, our analysis showed that, although the first derivatives at the surface are identical between the models, the second derivatives vary between each other. This will therefore ultimately lead to some divergence between the temperature profiles.

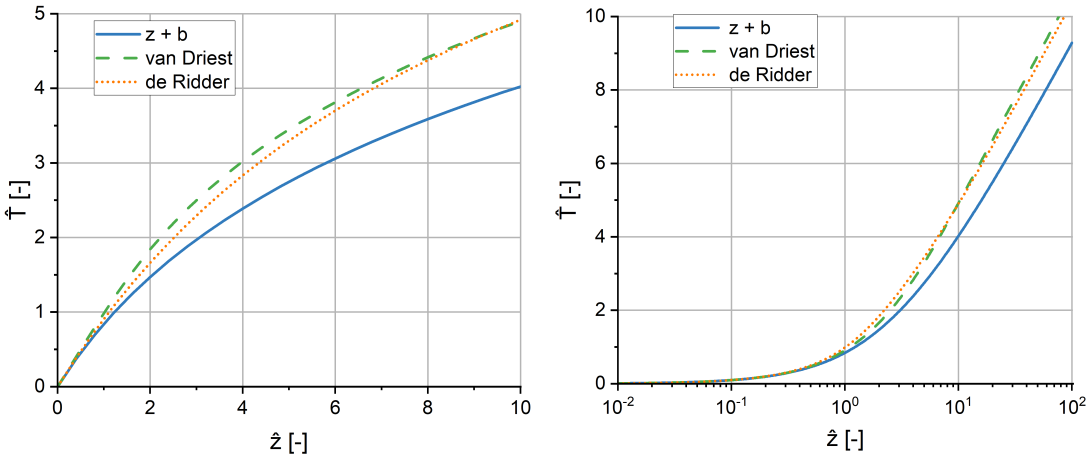

(a) (b)

Figure 3.2.: The numerically integrated profiles of the different models on a linear (a) and a logarithmic (b) scale.

In the end, these scaled models provide a way to compare the different models on the same surface based scale. The scaling steps also provide a method to scale future measurements to collapse in a similar way as these models.

4. Experimental methods

To analyse temperature profile behaviour near the surface, two measurement set ups were used: a set up designed by Jonathan Izett at Cabauw, the Netherlands [13, 14], and a set up designed by Judith Boekee at Veenkampen, also in the Netherlands[1]. From this point on, these will be referred to as the Cabauw case or the Veenkampen case. The Cabauw measurement campaign ran from the 3rd to the 22nd of November 2017, while the Veenkampen measurement campaign ran from the 1st to the 24th of May 2022. Both data sets use Distributed Temperature Sensing (DTS), but their specific execution differs slightly. The set ups will be explained and illustrated in section 4.1.

The two data sets undergo some pre-analysis steps. Section 4.2 details the different pre-processing and selection steps, the data analysis is then highlighted in section 4.3.

The Cabauw case is used to review the work done by Nollen (2022) [5] and we will take the same data pre-processing and selection steps as in his work. The procedure of this revision will be shortly summarised in section 4.3.

4.1. Measurement set up

Because both cases use DTS, it is important to understand the basics and specific needs of a DTS set up. DTS uses fiber optic cables, where the Raman scattering properties depend on the temperature of the cable [15]. The back scattered light is measured with a DTS machine (Silixa Ultima-S in Cabauw case and Silixa Ultima-M in Veenkampen case) to determine the temperature along the cable. For the measurements to be accurate, the set up needs temperature calibration in real time of the DTS cable. In both site cases, the cable temperature is calibrated by using two monitored well mixed water baths[2]. For the Cabauw case this meant first through a water-ice bath then an ambient temperature bath, the Veenkampen case had a continuously warmed and ambient temperature bath. The temperature further down the cable can then be inferred by the temperature in these baths and by the difference between these baths. These baths were placed at the beginning of the cable as well as at the end, to allow for double ended configuration.

After the cable passed through the calibration baths, there are two structures present in both cases: a tall mast and a secondary structure. Research proposes the use of 2D grid-like structures to increase the spatial resolution of the measurements, instead of just using a point based set up [16]. Both site cases try to use this idea. The execution of the secondary structure is different for each case, so they will explicitly be described per case. Figure 4.1 shows a photo of the Veenkampen set up of the mast and its secondary structure.

[1] The data set can, once published, be found via DOI:10.4121/21444063.

[2] Additionally, the python package "dtscalibration" was used for calibration. See: https://github.com/dtscalibration/python-dts-calibration

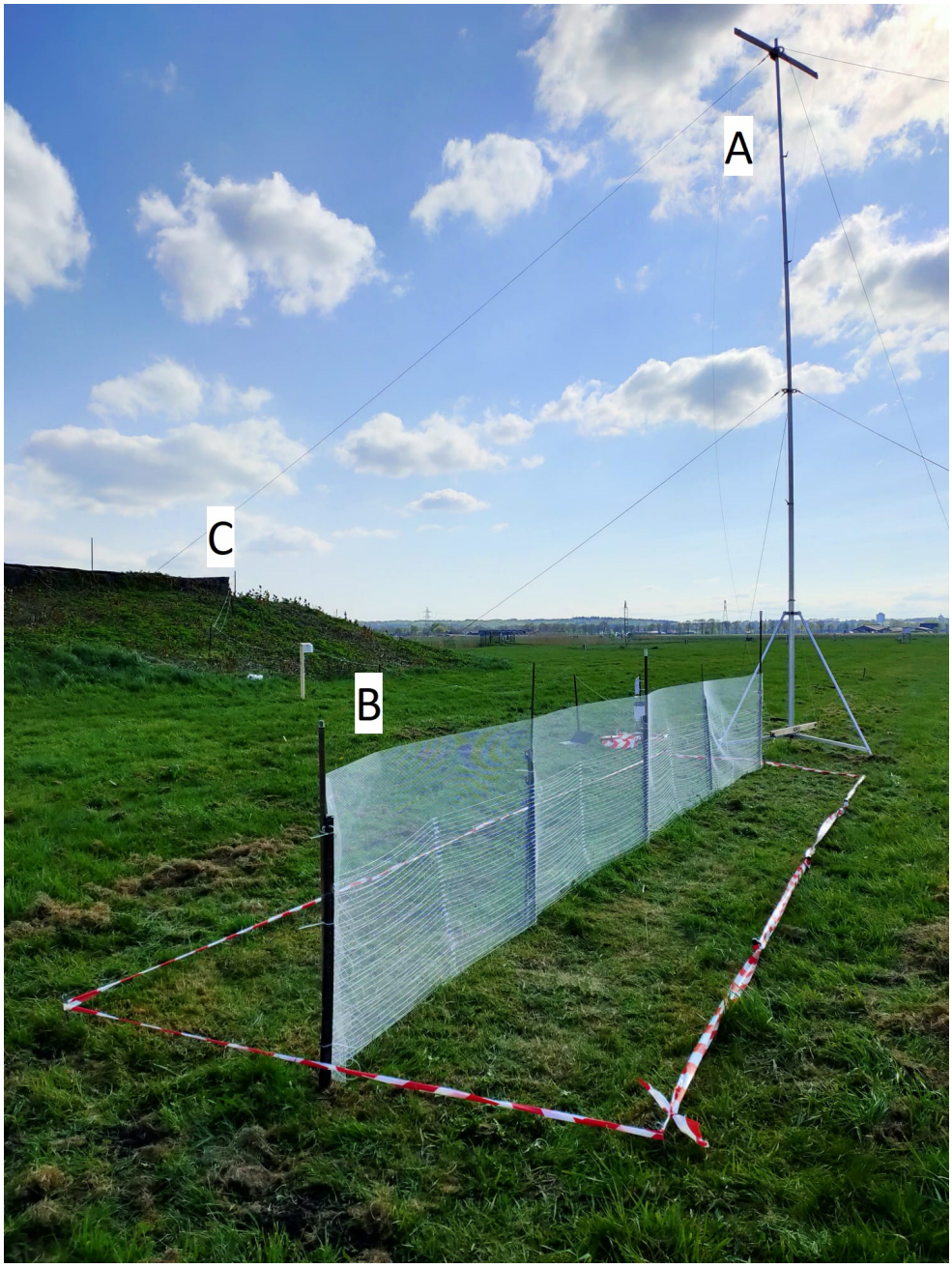

Figure 4.1.: A photo of the measurement set up of a mast and a secondary structure with DTS in a grassy field at the Veenkampen weather station in Wageningen. [A] is the pneumatic mast with the cables attached to wooden beams. Structure [B] is the secondary harp structure with the cables attached to a fibre glass mesh, the grass is maintained at the different heights in between the tape. The final point of interest [C] is where the cables lead to the DTS machine and logging computer contained inside the weather station. The other instruments visible are not used in this research. Photo taken by Judith Boekee.

The mast structure in both cases is designed to include the transition from the surface temperature profile to the logarithmic regime and thus needs to reach high above the surface. It consists of a pneumatic mast with two beams attached to it at an almost surface height and a top height. The DTS cable attaches to both ends of each beam, spanning the cable like a vertical rectangle. The fiber optic cable is a delicate instrument and can therefore not be fully fixated or it might break. The beams have foam tubes, through which the cables are clamped as tightly as possible. The configuration is schematically depicted in figure 4.2.

The second structure is, as mentioned, different per measurement set up. The set ups will be discussed separately below, explaining the secondary structure as well as some other key features that are site specific.

Firstly, the Cabauw case is set up differently from the Veenkampen case both by a coiled secondary structure as well as dry and wet fibre optic cables. The set up is located next to the KNMI CEASAR tower[3] on a grass field with grass height of approximately $h \approx 0.10m$. Izett[13] investigated the development of shallow fog detection and used the dry and wet cables to calculate relative humidity. In his research, Nollen [5] used the dry cable temperature of the Cabauw data set combined with the measurements of the KNMI at the same site. To review and reassess Nollen's work, we make use of the same data. The coiled secondary structure stands 1 meter tall and besides the mast of 7 meters tall. The cable follows a helical path to tighten the vertical resolution of the measurements from approximately 13cm down to approximately 1.5cm. Data of this measurement set up is summarised in table 4.1 and schematically depicted in figure 4.2.

The second site, the Veenkampen uses a 2D harp secondary structure with horizontal layers of cable over different grass heights. This set up was at the Veenkampen weather station of the Wageningen University. During the measurement period, the grass height was maintained in 4 sections with heights of 3cm, 10cm, 20cm and unrestricted, meaning that this grass was not cut, see figure 4.2. The surrounding grass was unrestricted, starting at a height around 10cm and continuing to grow to around 20cm. The so-called harp started at the soil surface and went up to almost 70cm high, spanning horizontal lanes of almost 8 meters long with a spacing of 2cm between each lane. Rather large horizontal sections were chosen in order to allow for horizontal averaging along sections of uniform grass height. This increases accuracy and can aid in analysis of the influence of different grass heights. The DTS cables were glued to a fiber glass mesh, to better maintain the alignment of the different lanes and their heights. A schematic illustration of the set up is depicted in figure 4.2 and an overview of the characteristics can be found in table 4.1.

Table 4.1.: Overview of the characteristics of the different measurement cases.

Characteristics	Cabauw site [14]	Veenkampen site
Mast range	0.07 - 7m	0 - 9m
Mast resolution	0.13m	0.3m
Secondary structure	Coil	Harp
Secondary structure range	0 - 1m	0.02 - 0.70m
Secondary structure resolution	0.015m	0.02m

Both data sets have a high temporal resolution, measuring continuously and saving data every 1 minute. DTS cable itself has a spatial resolution of more or less 13cm or 30cm,

[3]More information on this measurement tower from the Royal Dutch Meteorological Institute can be found at: https://www.knmi.nl/research/observations-data-technology/projects/cesar-cabauw-and-wind

see table 4.1. The difference between each measurement point will for each measurement instance be the same, meaning that the displacement between measured temperatures is more accurate than the exact location.

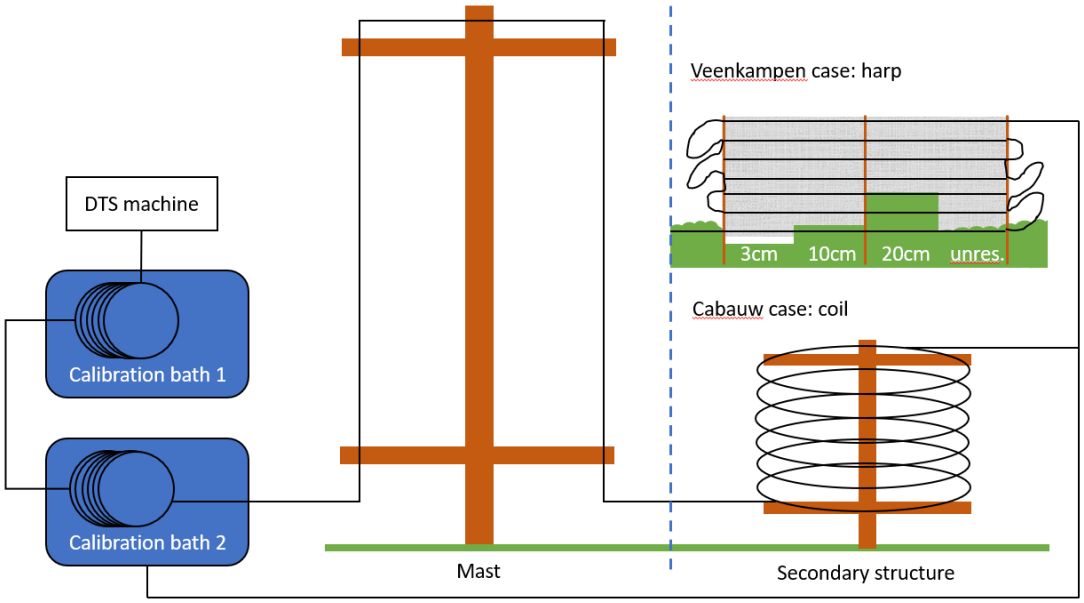

Figure 4.2.: Schematic drawing of the DTS measurement set up, both of the Cabauw case with a coil and the Veenkampen case with a harp. The values for the heights and spacings of the measurement structures can be found in table 4.1. In the Veenkampen case, the harp spans different grass heights: 3, 10 and 20cm and one part was left to grow unrestricted (unres. in figure). The DTS cable will on the way back pass through the calibration baths and into the DTS machine again, but this has been left out of the schematic for simplicity purposes.

4.2. Data selection

After the DTS data acquisition, averaging and selection steps will reduce the measurement data to useful data that can be analysed. This section will detail those steps.

Due to the chaotic nature of turbulence, the temperature averages are of interest in order to deduct mean-temperature gradients. In the case of the Veenkampen, the average temperature over the same grass height is taken. For this spatial average, the edges between the different layers are omitted, as the transition area could influence the flow and mixing above it. This means that the measurement points around the transition areas were left out of the averaging step. The other averaging step is over time. This was done after the spatial averaging in the Veenkampen case. Both cases are averaged by a moving average over 10 or 30 minutes, with 10 minutes the averaging time for most of the data analysis, unless stated otherwise.

The next step after averaging is selecting the data for further analysis, which is based on 3 criteria: smooth and monotonic curves, logarithmic behaviour, lack of precipitation. The goal is to use fully developed and representative temperature data, where these criteria exclude the non-stationary or transient periods in the data. The criteria are implemented as follows below:

1. **Smooth and monotonic curves** exclude most of the remaining turbulent structures in the data. The averaging step should provide smooth and monotonic data where the chaotic nature of turbulence has been diminished. It is, however, still possible that non-stationary mean temperature profiles appear after the averaging step if there was too intense mixing during that time step. This would be a sudden deviation of the overall curve, expressing as a bump in the curve. These periods should be excluded. The useful data should be mostly monotonic, meaning no sign changes in the first derivative. Figure 4.3a shows an example of a non smooth and non-monotonic curve that would be excluded. During this research, this criterion was visually checked for in the selection process.

2. Higher above the surface **logarithmic behaviour** appears both in theory and the models developed in chapter 3, and are accepted in literature with vast observational evidence. Representative data should therefore exhibit this logarithmic behaviour in the top of the data range. The temperature profile would vary from this logarithmic behaviour during transitional periods from stable to unstable regimes or vice versa, or during rapid changes in the weather conditions. These transitional periods are out of scope for this research, therefore finding logarithmic behaviour in the upper part of the measurements is key. The data is plotted on a logarithmic scale and the data between 4m and the top of the mast is visually compared against a line or ruler. Figure 4.3b shows an example of a curve with a straight and smooth line in the upper regime of the mast data.

3. **Precipitation** is another factor that would highly influence the atmospheric properties and is in this thesis excluded. Using data from either the KNMI Cabauw or the Veenkampen weather stations, we checked the interesting periods of the data for precipitation. Precipitation was checked around the 10 minute averages with a margin of another 10 minutes, resulting in checking 30 minutes of data for precipitation profile of interest.

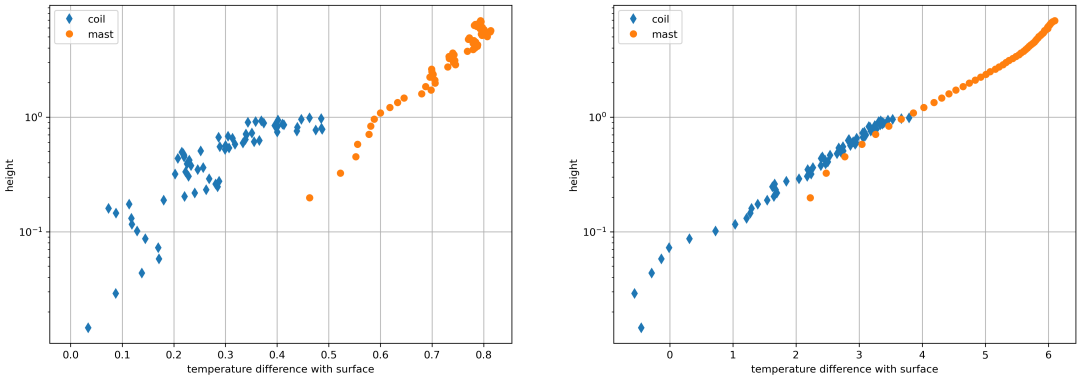

(a) (b)

Figure 4.3.: Examples of the data that is put through the selection criteria showing coil (blue diamonds) and mast (orange circles) data. (a) will be excluded by the criteria as is not fully smooth and even non-monotonic both in the coil and mast data. (b) will be included as it is a very smooth curve with a clear logarithmic regime in the upper part of the mast data. Data from Cabauw.

We compared the data like that in figure 4.3 and selected the data based on the criteria above for both stable and unstable cases. This research focuses mostly on stable cases, but will include some exemplary unstable cases. The selected data will, after checking for these criteria, resemble the profile like that in figure 4.3b.

4.3. Data analysis

The first step in the data analysis is building upon the work of our predecessor, Paul Nollen [5]. Firstly, data analysis will focus around recreating and reviewing his work, which states once again that the definition of z_{0h} is non-robust and finds that the measurements often show a constant gradient near the surface. He also introduces the length scale b, which in this case is of the order of half the grass height. All analysis on the Cabauw data will be for the revision of his work and will resemble his method.

Figure 4.4 shows the major steps taken in the analysis of Nollens work. The surface temperature was taken to be the temperature at the lowest point of the coil data. In the higher regions the mast data points organise along a straight line: the logarithmic range. In the traditional approach, this log-regime is extrapolated towards the surface (dashed line in figure). The intersect with the surface temperature (the vertical blue line in the figure) then defines the roughness length z_{0h}. This characteristic height is in figure 4.4 denoted by the red horizontal line. The boundaries of the logarithmic regime were visually determined for each case, see the crosses in the figure.

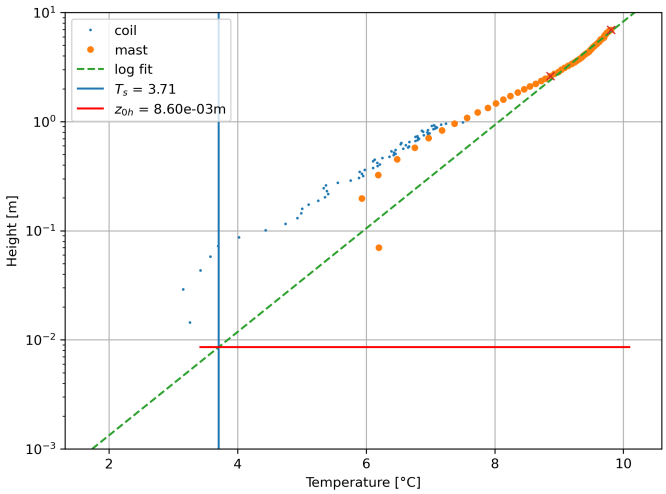

Figure 4.4.: An example of temperature profile from the Cabauw case on a logarithmic scale. The thick orange markers are the data points from the mast, the thin point markers are the coil data points and the dashed line is the extrapolated logarithmic profile through the upper part of the mast data points, which has been plotted on the area between the crosses. The other plotted lines are the measured surface temperature (vertical) and the subsequent roughness height z_{0h} (horizontal).

The second step of the data analysis investigates the viability of the framework proposed in chapter 3. This step uses the Veenkampen data and further details of the methods will use the Veenkampen data above a representative constant grass height for the larger surrounding area, being 10cm for the first period of the measurement campaign.

4.3.1. Scaling

This section details the steps taken to analyse the experimental data in the proposed framework in chapter 3. Both the temperature and height of the experimental data will be scaled.

The first analysis step is to determine the turbulent heat flux scale θ_* and scale the temperature using $\hat{T} = T/\theta_*$. To determine θ_*, following Eq. 2.1, we take two points in the logarithmic regime and then $\theta_* = \kappa(T_2 - T_1)/(ln(z_2/z_1))$. Points 1 and 2 were taken at mast heights of 3.8 and 7.1m. These points are indicated in figure 4.5

Next, we will deduce the "surface length scale" $\mathcal{L}_s$ as to normalise and scale the height coordinate. $\mathcal{L}_s$ depends on the surface temperature gradient and θ_*. The closest points to the surface were irregular, so points from 0.062 to 0.169m harp height were used to determine the slope of the temperature, see figure 4.5. This larger range was chosen as to exclude the influence of the grass on the heat flux and have points both in and above the grass. A line was best fitted through the points in this range, from which the slope was then used to determine the length scale $\mathcal{L}_s$ via eq. 3.2. This was then compared against an a priori determined constant length scale κb, based on Nollen's research. Nollen used $b = 1/2 \cdot h$ with h the grass, in this research the κb will be dependent on the grass height as well, which will be verified in chapter 5. Its final value will be compared from the results for $\mathcal{L}_s$. As the aim of this research is to find one parameter based on the surface geometry, we will work with a constant value for $\mathcal{L}_s = \kappa b$. Using $\hat{z} = z/\mathcal{L}_s = z/\kappa b$ will then finally result in the final scaling of the data.

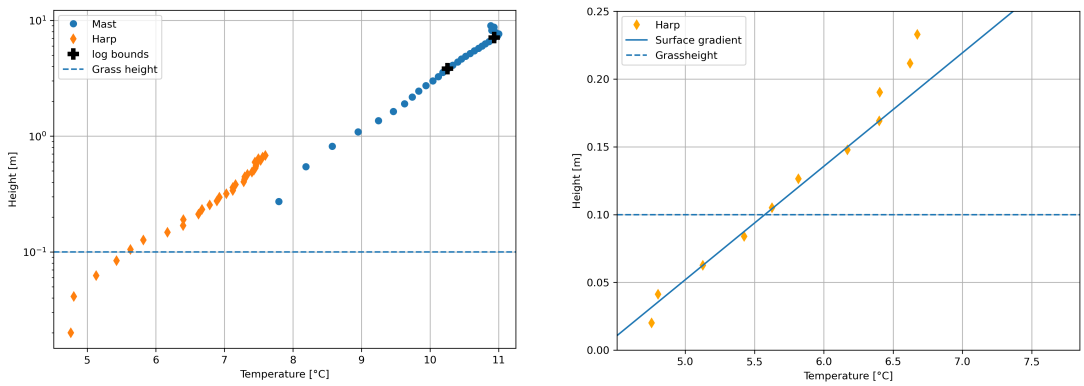

(a) (b)

Figure 4.5.: Step for the determination of the scaling parameters: two points (+) in the logarithmic regime for the determination of θ_* (a) and the line fitted through the surface points for the determination of $\mathcal{L}$ (b). Note that the left figure is on a logarithmic scale, where the right is on a linear scale. Data from the Veenkampen case.

Even if the data is scaled, individual measurements might be subject to case-specific disturbances, such as advection or other turbulence effects. By constructing a composite of multiple cases and averaging those, we expect that case-specific deviations are diminished. We can then assess the general physical behaviour. These composites will be called categories and are made according to subsets of θ_* values of the selected data points. Unstable

instances will have a negative value of θ_* and will be their own category. For the stable cases, the subsets are chosen such that the number of cases in each category is similar.

To compare the scaled data to the models derived in chapter 3, the data and models should be plotted at the same level and not be displaced by their individual surface temperature. In this thesis, we specifically use a characteristic length scale from the surface for the scaled models and data. We aim to find a unified profile of the data at the surface and thus use a reference temperature T_{ref}. Instead of finding the scaled temperature like $\hat{T} = T/\theta_*$, it is calculated with $\hat{T} = (T - T_{ref})/\theta_*$. However, it is unclear at what height the correct temperature for T_{ref} should be taken. Figure 4.6 shows a close up of the set up near the surface. The grass is highly variable in density horizontally, but especially vertically. The temperature profile will depend on the heat absorbed or released by the grass, so the apparent surface of the atmospheric temperature profile depends on the grass. This research will perform a sensitivity analysis where we determine the reference height at which T_{ref} should be taken. For the sensitivity analysis, we take 3 different measurement heights at which we determine

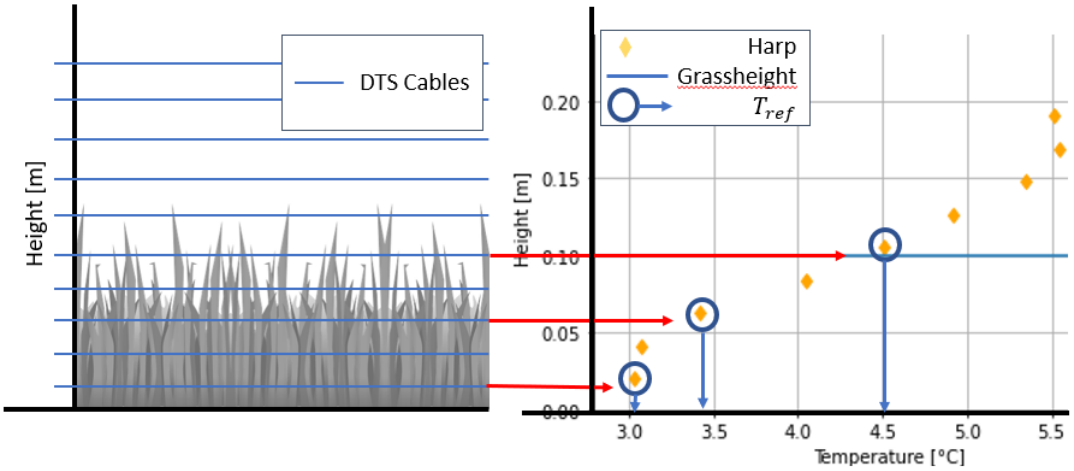

Figure 4.6.: On the left an illustration of "realistic grass" with the DTS cables through it. The right side shows an example of a measured profile where the approximated top of the grass is indicated. Different choices for the reference height (for example the red arrows) can be made, which would on the right translate to a different T_{ref} (circles and blue downwards arrows).

the temperature and take that as T_{ref}. The height of the data is determined with respect to the soil surface, in figure 4.6 this is depicted as the bottom of the figure on the left. On the right side, we see one example measured profile with the estimated top of the grass height indicated. This figure illustrates the choice for T_{ref} from the different heights. The data was subtracted by the temperature from the lowest harp measurement point $z = 0.02$, the temperature at half the grass height $z = 0.063$ and at the top of the grass $z = 0.105$.

4.3.2. Model verification

The research closes with a short investigation towards the ability of the models to describe the observed profiles followed by analysis of their predictive qualities. In chapter 3, we saw that the gradients of the proposed models show more differentiation than their profiles do, see figures 3.1 and 3.2. This difference could be indicative of the ability of the models to describe experimental data. The gradient of the data is calculated via two point numerical differentiation. Afterwards, the models are then compared to this experimental data. We will use the reference height determined in the sensitivity analysis as the "surface height" for the models.

To investigate the predictive qualities of the models, we test the predicted surface temperature versus the measured temperature. To arrive at these temperatures, we take a couple of steps. Figure 4.7 shows an example of what the result of this process would look like. Firstly, two points in the logarithmic regime are used to determine θ_*, which then scales these points via $\hat{T} = T/\theta_*$. Next, the tested models are aligned with these points, meaning they are displaced by the scaled temperature at these heights. Afterwards, the model is extrapolated towards the scaled reference height (the height at which T_{ref} should be taken which is likely the apparent surface) and the scaled surface temperature is recalculated to an actual surface temperature $T_{s,\text{prediction}}$, see figure 4.7 for an illustration of the resulting process. The Root Mean Square Error (RMSE) is then calculated by using the actual measured surface temperature $T_{s,\text{measured}}$ via

$$\text{RMSE} = \sqrt{(T_{s,\text{prediction}} - T_{s,\text{measured}})^2}. \tag{4.1}$$

The lower this RMSE (with the same units as the temperature [$^\circ C$]) is, the better the model performed at determining the surface temperature. A model would be better at predicting surface temperatures if it consistently had a lower RMSE in this analysis.

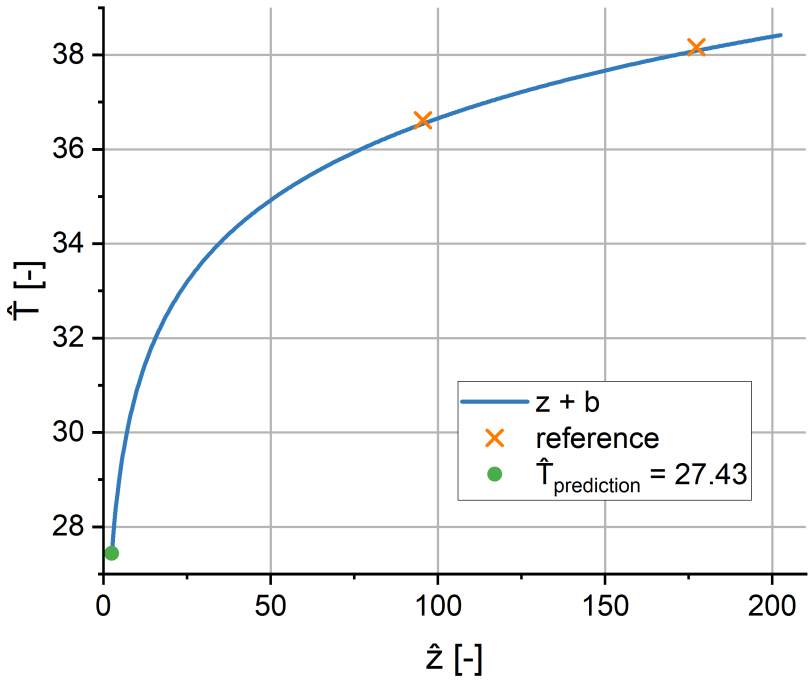

Figure 4.7.: Example of the result of the process of predictive quality analysis, where the predicted surface temperature $\hat{T}_{s,\text{prediction}}$ is determined. The crosses are 2 scaled data points in the logarithmic regime, the model (in this case the z + b model, but this works similarly for the other models) is then fitted through these points and extrapolated towards the height at which T_{ref} (the dot) should be taken.

5. Results

This chapter will present the main results from each research step during this thesis. After the short review on Nollens work with Cabauw data, the Veenkampen data has been used for further analysis of the temperature profiles just above the surface. Further interpretation and discussion of the results will be in chapter 6.

5.1. Review of work by Nollen

Recreating Nollens work on the Cabauw case resulted in temperature profiles like figure 5.1. The 4 timestamps all show logarithmic behaviour in the upper regime and then start to differ from the classical MOST model as the measurement points are nearing the surface. The coil data shows further deviation from the model than the mast data does on the same height. Nollen saw this same discrepancy between the MOST model and the data, where he distinguished a new regime that followed another slope with logarithmic behaviour. The calculated roughness height for the four timestamps is respectively $z_{0h} = 5.1 \cdot 10^{-6}; 9.0 \cdot 10^{-5}; 4.6 \cdot 10^{-2}$ and $5.4 \cdot 10^{-5}$m. This is a spread of 5 orders of magnitude. Note that by this procedure a very small error in the slope immediately translates in a large change of the roughness length z_{0h}, especially visible in the third plot of figure 5.1.

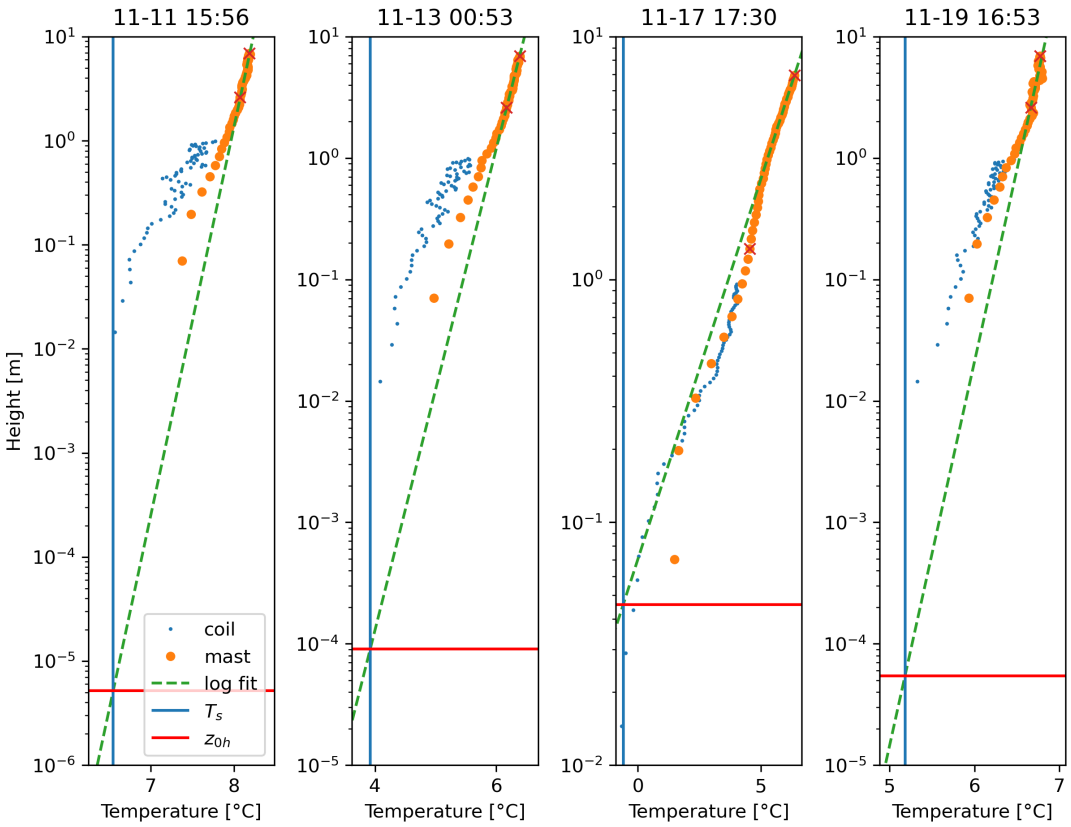

Figure 5.1.: Four different time stamps of the measured temperature with the mast (large markers) and coil (thin markers) of the Cabauw case plotted with a logarithmic scale y axis for the height. In each plot, the classical model is plotted with a dashed line through the upper part of the mast data and the surface temperature is plotted as a vertical line. For each plot the roughness heights are plotted with a horizontal line, except they can be outside the scope of the graph. From left to right the values of the roughness heights are $z_{0h} = 5.18 \cdot 10^{-6}; 9.01 \cdot 10^{-5}; 4.58 \cdot 10^{-2}$ and $5.43 \cdot 10^{-5}$.

5.2. Scaling the data

After the data selection for the Veenkampen case, 36 instances of 10 minute averages were found, from which 2 unstable cases and 34 stable cases. These cases were between the period of 4th of May 00:00 and 13th of May 23:59, the grass height in the area surrounding the measurement set up was approximately 10cm during this period. All cases were found to have a logarithmic regime between heights of 3.8 and 7.1m. The exact timestamps of the selected instances are found in appendix B.

As an example of the Veenkampen data, figure 5.2 shows one instance of the averaged temperature profile. There are 3 key features to note: (1) the gap between the mast data and the harp data, where the top of the harp temperatures increase at a lower rate than the mast data at the same height does; (2) the lowest harp measurement points seem to not follow the trend of the other measurement points and between other instances there does not seem

to be a recurring behaviour, these points are inside the grass and it is expected that heat is transported differently here; and (3) the top of the mast is inverting with respect to the data below.

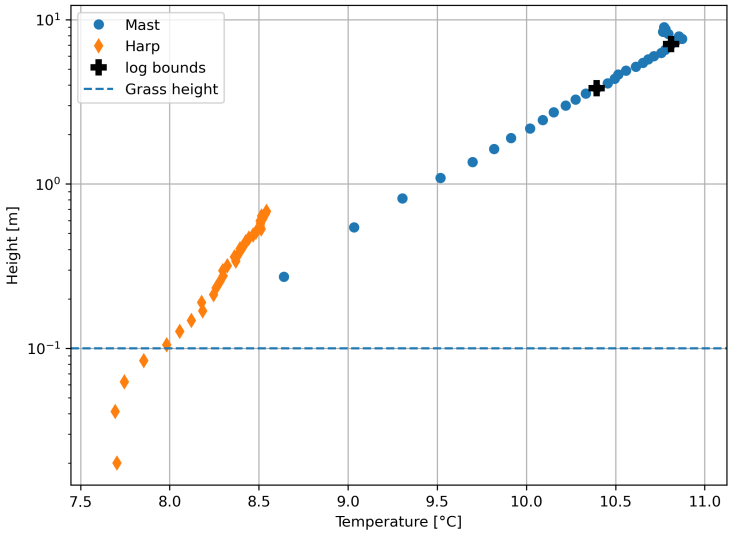

Figure 5.2.: 10 minute averaged temperature profile of the Veenkampen case of both the mast (circles) and harp (diamonds) data. The crosses (+) indicate the edges of the logarithmic regime for this data instance. The horizontal dashed line is the grass height.

At first, the scaling parameters for each instance were calculated following the indications in figure 4.5. The resulting values for the scaling parameters can be found in figure 5.3. In the instances found during this research, the turbulent heat flux scale θ_* varies between $-0.2°$ and $0.8°$, with the most data having a θ_* value of $0.3°$.

The next scaling parameter, the length scale $\mathcal{L}$, has values between 0.01m and 0.09m, with a mean of 0.043m. The values of $\mathcal{L}$ are within 1 order of magnitude. Chapter 3 showed that the length scale of the z+b model should be $\mathcal{L}_b = \kappa b$. In Nollen's thesis, he proposes $b = 1/2h_c = 0.05$m, but this is a different parameter from the length scaling parameter. If we then use $\mathcal{L}_b = \kappa h_c = \kappa \cdot 0.10 = 0.04$m and compare this to the results in figure 5.3b, we see this is close to the mean of the actual surface gradient based length scale.

With the scaling framework, the models in chapter 3 can be compared to the experimental data. Figure 5.4 shows an example of a single observed scaled temperature profile $\hat{T}(\hat{z})$ compared against the various models. The models have for illustration purposes been vertically displaced to align with the lowest data point. As this is a single example only, the generality of the model descriptions will be assessed against the full data set in the following section.

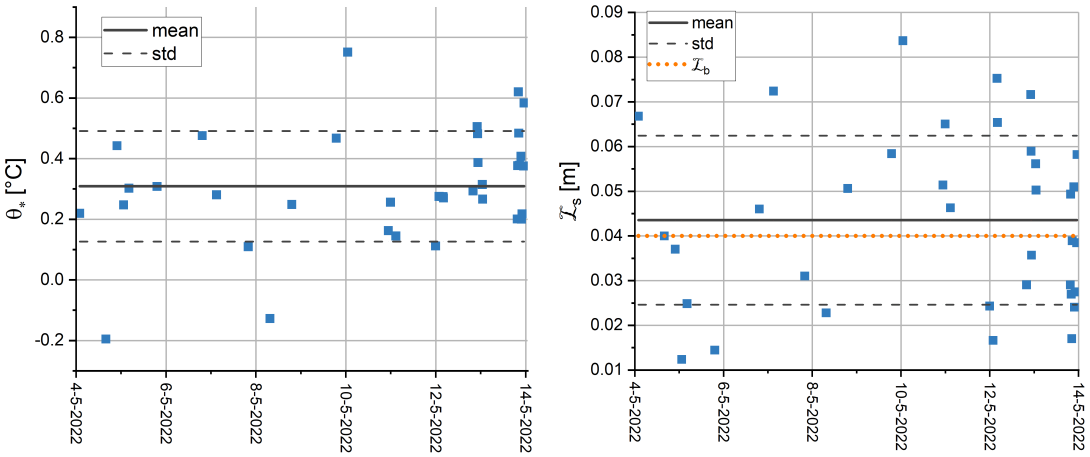

(a) (b)

Figure 5.3.: The scaling parameters for each separate time interval. (a) the turbulent heat flux scale θ_* determined with 2 points within the logarithmic regime. (b) the different length scales $\mathcal{L}_s$ determined by the surface length with the mean (line) and standard deviation (dashes). The dotted line is the value of $\mathcal{L}_b = \kappa b$ used during this research.

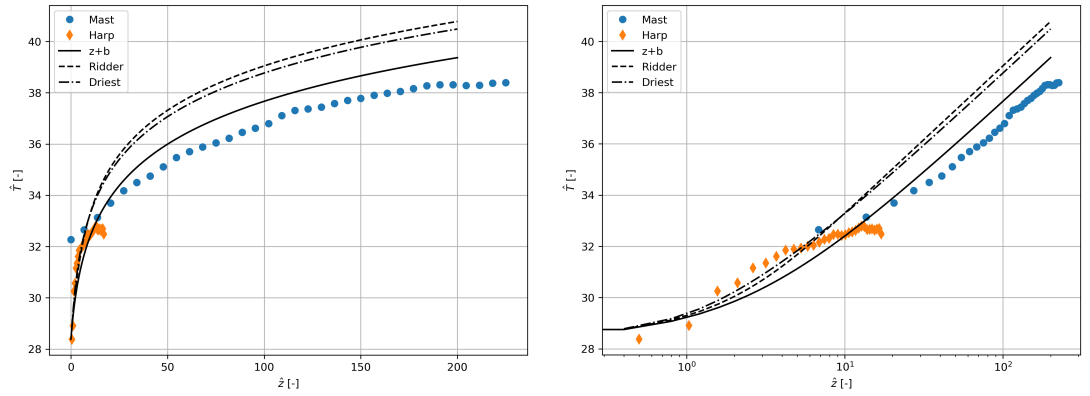

(a) (b)

Figure 5.4.: Example of scaled stable temperature profile with scaled $\hat{T}$ and $\hat{z}$ on a (a) linear scale and a (b) logarithmic scale. The circles are the mast data points and the diamonds are the harp data points. The dark lines are the models that have been vertically displaced by the temperature value of the lowest measurement point and are plotted until $\hat{z} = 200$.

5.3. The temperature scale categories

To analyse the temperature profile behaviour in a more general perspective, the scaled instances are categorised based on stability and θ_*. This resulted in 5 categories, summarised in table 5.1. The average profile of each category is given in figure 5.5. If the scaling framework was perfect all average profiles should have a similar shape. This seems to be indeed the case. The off-set is a result of the difference in surface temperature. In order for the curves to collapse, surface temperatures would have to be subtracted. For an initial comparison of the scaled models and the experimental data, figure 5.5 depicts the models as well. The models have a similar overall shape as the data, yet they are not fully overlapping.

Table 5.1.: Overview of the different categories, their range and the amount of instances in each category.

Category	C0 (unstable)	C1	C2	C3	C4
Range	$\theta_* < 0$	$0 < \theta_* < 0.25$	$0.25 < \theta_* < 0.3$	$0.3 < \theta_* < 0.45$	$\theta_* > 0.45$
Instances	2	10	6	9	8

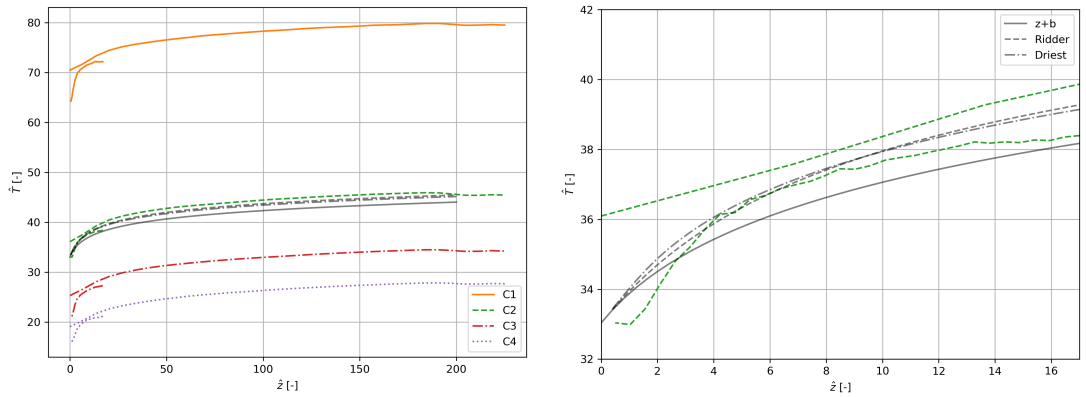

(a) (b)

Figure 5.5.: The mean of the temperature profiles of the harp measurements for the different stable categories of all the categories (a) and zoomed in on the harp data from the C2 category (b). The names of the categories correspond to those in table 5.1. The grey lines are the 3 models, see legend of (b), that have been displaced by the value of the C2 category mean at $\hat{z} = 0$.

As the categories are not overlapping in figure 5.5, we investigate the profiles with different reference temperatures T_{ref}. As it is not a priori obvious at what height the representative surface temperature is, we present 3 cases as indicated in section 4.3. The results from this sensitivity analysis are shown in figure 5.6.

For the data that have been displaced by the temperature at 2cm height, which is almost considered the ground (figure 5.6a), the scaled profiles for each averaged category are spread out. For the other cases where the displacement temperatures are taken at 6cm, being half the grass height, (figure 5.6b) and 11cm, being height of the top of the grass (figure 5.6c), the curves start to converge until they collapse onto each other. The profiles do start to diverge

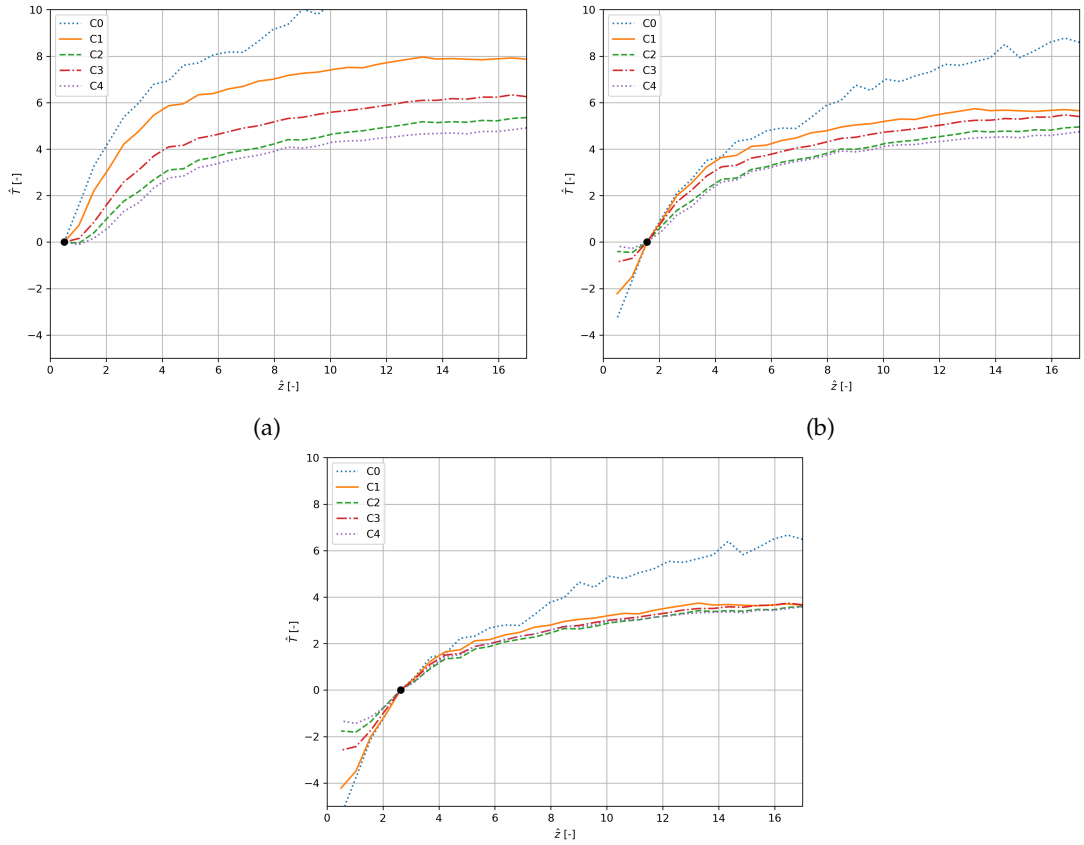

Figure 5.6.: Average of the scaled data per category with reference temperature T_ref at different heights: (a) 2cm, (b) 6cm and (c) 11cm which is the top of the grass height. The categories correspond to those in table 5.1, where the top blue dotted line is the mean of the unstable cases and the others are the stable categories. The black dot is the reference point that has been used to displace the different profiles.

below the displacement height. The physical heights $z = (0.02; 0.06; 0.11)$m are scaled to $\hat{z} = (0.5; 1.5; 2.5)$ respectively. In each of these figures, the unstable category has a different profile shape than the stable categories, but this profile was only based on 2 instances and needs further separate research.

Most importantly, the stable temperature profiles overlap each other in 5.6c. This means that in the Veenkampen case, a representative surface temperature should be taken at the top of the grass at $z = 0.11$m or $\hat{z} = 2.5$.

5.4. Model verification

In the end, we want to compare the data to the models derived in chapter 3. For this we investigate the gradients of the data, as the models show more differentiation in their gradients. The two-point gradient of the data is plotted in figure 5.7. The figure shows that the gradient starting from the ground, first increases to larger than 1 and then, while passing the top of the grass height at $\hat{z} = 2.5$, decreases where it becomes small for larger scaled height. Figure 5.7b particularly shows that the calculated gradient of the harp does not have a smooth gradient.

The models are plotted starting from the height determined as the representative surface height, at $\hat{z} = 2.5$. For the harp data, no particular model seems to align best, while all models converge to the mast gradient data as $\hat{z}$ increases. The models overlap with the mast data down to around $\hat{z} = 15$, which is about 0.6m above ground.

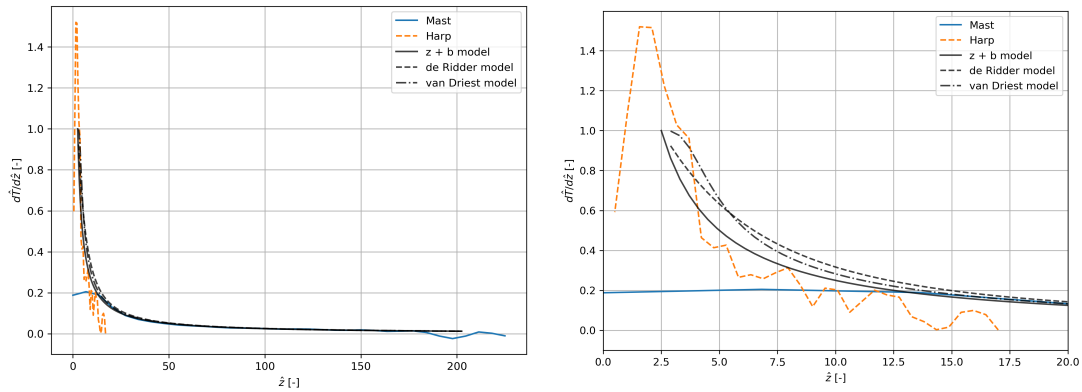

(a) (b)

Figure 5.7.: The two point calculated gradient of scaled data, the full measurement range in (a) and a close up of the harp data in (b) with the models plotted to start at $\hat{z} = 2.5$.

Another verification pathway is by use of the predicted surface temperature RMSE for each model, for which the results are shown in figure 5.8. The range of the errors spans 3 orders of magnitude, with the lowest errors at 0.008°. Except for the exceptionally high error for the $\theta_* = 0.75°$ instance, all errors are smaller than 2° but most are even smaller than 1°. The actual amounts of RMSE per model that are smaller than 1° is 82% for $z + b$ model, 68% de Ridder model and 76% van Driest model. This means that each model, with the use of the framework, would be able to predict the apparent surface temperature within less than 2° accuracy. There is, however, no clear model that consequently has a lower RMSE for the predicted surface temperature.

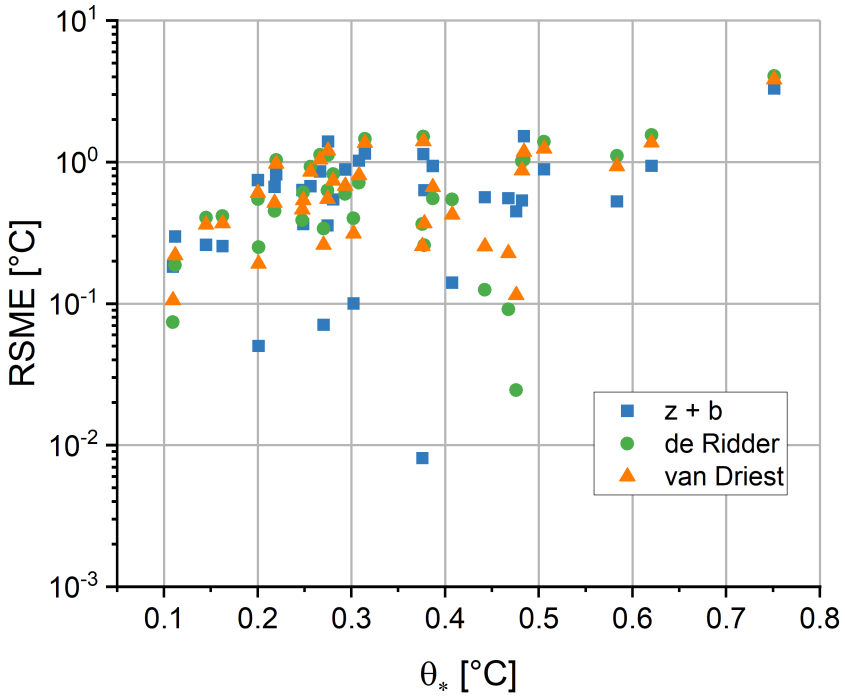

Figure 5.8.: RMSE in prediction of the surface temperature at 11cm using the $z + b$ model (squares), the de Ridder model (circles) or the van Driest model (triangles) versus the turbulent heat flux scale θ_*.

6. Discussion and recommendations

During this research, a new framework for theoretical models was developed and examined with experimental data to try and verify what model could be used to accurately describe the near-surface temperature profile. This chapter presents the interpretation of the method and results. Afterwards, the recommendations to improve on the research for each part are presented.

The Distributed Temperature Sensing (DTS) measurements provided high spatial and temporal resolution data. Its representative data points could be used to calculate the scaling parameters and compare the data. Both the Cabauw and the Veenkampen measurement set ups provide temperature profiles useful for our analysis.

Figure 5.2, however, shows several unexpected patterns for the Veenkampen data. Both Schilperoort et al. [15] and Thomas et al. [16] describe possibilities and limitations for DTS air temperature measurements. The patterns in the found profiles could be explained by these limitations. The most prominent pattern is the gap between the mast data and the harp data. Eventhough the models can overlap with the bottom part of the harp and the upper part of the mast, for the transition from harp to mast it is unclear what the profile should exactly look like.

One explanation of the gap between the mast and harp structure could be that they cool or warm differently. DTS cables cool and heat up by the wind and sun [15]. It is uncertain how the cooling and heating of the cables exactly works in either the mast set up or the harp set up. If the cables are heated or cooled, they have a different temperature from the actual air temperature. This could mean that the gap in the measured profiles is because the cables at the top of the harp or at the bottom of the mast are not actually at air temperature.

Another explanation is that the actual height of DTS measurements is often difficult to determine and the lowest mast points are actually on a different height. The relative height of the measurement points on the cables are better established. This means that the gradients in the temperature measurements are better defined, which we use for the calculation of the scaling parameters. The uncertainty in absolute height could, however, explain the gap between the mast and harp as well as the top of the mast inverting. There is furthermore the possibility of the cables of the mast slipping through the clasps and the harp top lines sagging. This could mean that the temperature points are plotted at lower or higher altitudes than they should be.

To mitigate this uncertainty in the DTS measurements, the set up could be redesigned to lessen the cooling or heating effects by wind or sun, see [15] for ideas. On the other hand, by using additional shielded temperature sensors at certain heights to determine the actual air temperature, the heating and cooling effect could be quantified and excluded in the DTS measurements. Another possibility to increase the certainty of the DTS measurements could be to create one overall structure where height is well defined over the full spectrum, Thomas et al. [16] developed a set up that covers an 8 by 8 meters vertical grid that could be modified to define the height of the measurements better.

During this thesis, data selection was based on visual comparison. This is a subjective selection method that in this research resulted in 36 data points over a period of 9 days. Most data points were stable cases, as the mixing in this case is reduced and the temperature profile exhibits less thermal fluctuations [2]. Only 2 of the data points were unstable cases, as a first impression, but does result in a different profile from the stable cases. Because this thesis aimed to investigate the possibility of the framework, the current data set was sufficient.

Statistical significance in further research would require a larger data set obtained with an objective selection method. The current criteria would need to be defined more clearly and qualitatively for automated data selection. Automated data selection is not only an objective selection method, but could also help in gathering more representative data points.

Taking the comments on the measurement set up and the data selection procedure into account, this thesis still leads to one main result: a scaling framework that could potentially universally describe near surface temperature profiles. The framework and scaling steps developed in chapter 3 show that empirical models for high canopies and grass cases as well as Direct Numerical Simulation (DNS) models for smooth pipe flow can be compared on the same level. We showed that the temperature gradients all have a similar gradient and profile, with the biggest difference in the slope of the gradient at $\hat{z} = 0$. This also emerges in the slopes of the integrated profiles, where this will result in an offset at higher altitudes.

The models align with the scaled and averaged data in section 5.3, which shows that this could provide steps towards a universal model for the surface temperature profile. Where the temperature scaling of $\hat{T} = T/\theta_*$ is similar to that in MOST [2], the newly introduced surface length scale $\mathcal{L}_s$ seems to connect surface gradients and the surface geometry, see eq. 3.2. Using a reference temperature T_{ref}, this scaling leads to a state where the averaged stable profiles of different categories will overlap in figure 5.6. This points to the need to redefine the used surface temperature in models, the apparent surface for the heat mixing should not be considered at soil level or the roughness height z_{0h} which is on the order of less than 10^{-3}. This thesis indicates that the apparent surface temperature could be dependent on the geometry of the surface vegetation.

When using this framework to compare the models to the data, no particular model aligned fully with the data profiles or their gradients nor did any model perform better in the predictive capability testing in section 4.3.2. This could be because of the DTS aberrations mentioned before as well as the models not fitting the surface temperature profile. Additionally, the gradient of the data showed wiggles, which makes for difficult comparison to the models.

Future research could use different models like that of Harman & Finnigan for tall canopies [17] with the proposed framework. Using different models could also help in the physical understanding of the processes that lead to the actual temperature profile. Another recommendation step would be to develop the measurement set up, such that the gradient of the data profiles can be smoothed for comparison against the models. The models show immediate differentiation in their gradient slopes, which would be interesting to find in data.

When developing the framework and the use of the reference temperature, it should be noted that this apparent surface could possibly also depend on the solar radiation angle. Hicks and Eash [18] have found that the soil surface temperature and the air temperature at 2m above the surface differ more as the sun rises. They attributed this difference in heating to the height of canopy (in their case maise) and possibly to the canopy structure. More

direct sunlight heats the surface of the different canopy components, which in turn has an effect on the heating of the air. When continuing research in the proposed framework from this thesis, taking the effect of the solar radiation angle into account during analysis is important.

This research analysed the temperature profile above grass, similarly to Nollen [5]. Grass has a high variability in its structure and this will influence the flow and mixing through it. Dong et al. [19] show that displacement height d and parameters based on the displacement height are dependent on density and height of vegetation, so this will probably hold for the surface length scale $\mathcal{L}_s$ and the subsequent reference temperature T_{ref} as well. Performing the same measurements and analysis above different types of vegetation would be needed to finalise investigating the universality of the framework.

7. Conclusion

This thesis aimed to find a universal model for the near surface temperature profile. It reworked 3 different models (DNS smooth pipe [11, 12], tall canopy [9] and above grass [5]) in a scaling framework that would collapse the models at the surface. We measured the near-surface temperature profile using Distributed Temperature Sensing (DTS) in Veenkampen, Wageningen from the 1st to the 24th of May 2022. In total, 34 instances of stable and 2 instances of unstable temperature profiles were scaled in the same framework. These were categorised and compared to the models, both the profiles as well as their gradients.

Our scaling framework is able to connect thee different types of models, two experimentally developed and one Direct Numerical Simulation (DNS) validated, to the data in a universal profile. The framework used scaling parameters for the temperature $\hat{T} = T/\theta_*$ and $\hat{z} = z/\mathcal{L}_s$. The surface length scale is a possible parameter based on surface gradients $\mathcal{L}_s = \theta_*/(\partial T/\partial z)_{z=0}$ and connected to surface geometry $\mathcal{L}_s = \kappa b$. In the Veenkampen case this length scale was almost half grass height of 4cm. Once the data was then displaced by a reference temperature T_{ref} the scaled data points would collapse onto one profile if T_{ref} was taken from the top of the grass height at 10cm.

The comparisons to the models showed some promising overlap in the lower regime of the harp data, starting from the height of T_{ref}, and upper region of the mast data. However, no model overlapped fully with the profiles or the two-point gradient of the data. There was a gap between the mast and harp DTS data, which could be due to heating of the cables or perhaps the uncertainty in the actual physical height of the measurement points. This adds to the uncertainty of the alignment of the models to the data. In the verification effort of trying to use the models to predict the reference surface temperature T_{ref}, the error in the predictions for each models was less than 2°C but often even smaller. No model performed better overall than the others. This study can therefore not yet determine a final model that describes the near surface temperature profile.

Future research could through improved measurement set up and automated data selection attempt to find more convincing evidence towards one of the proposed models or different models from literature like Harman & Finnigan [17]. Furthermore, it could be useful to analyse the predictive qualities of the models and framework and investigate the prediction sensitivity to θ_*. It is finally recommended to test the framework in different vegetation cases for universal applicability.

Bibliography

[1] A. A. Holtslag, G. Svensson, P. Baas, S. Basu, B. Beare, A. C. Beljaars, F. C. Bosveld, J. Cuxart, J. Lindvall, G. J. Steeneveld, M. Tjernström, and B. J. V. D. Wiel, "Stable atmospheric boundary layers and diurnal cycles: Challenges for weather and climate models," *Bulletin of the American Meteorological Society*, vol. 94, pp. 1691–1706, 11 2013.

[2] A. F. Moene and J. C. van Dam, "Transport in the atmosphere-vegetation-soil continuum," 2014.

[3] P. G. Duynkerke, "The roughness length for heat and other vegetation parameters for a surface of short grass," *Journal of Applied Meteorology*, vol. 31, pp. 579–586, 6 1992.

[4] E. Vignon, C. Genthon, H. Barral, C. Amory, G. Picard, H. Gallée, G. Casasanta, and S. Argentini, "Momentum- and heat-flux parametrization at dome c, antarctica: A sensitivity study," *Boundary-Layer Meteorology*, vol. 162, pp. 341–367, 2 2017.

[5] P. Nollen, "The thermal roughness length: study on a mysterious concept," 2022.

[6] F. T. M. Nieuwstadt, B. J. Boersma, and J. Westerweel, *Turbulence Introduction to Theory and Applications of Turbulent Flows*. Springer Publishing, 2016.

[7] H. Jonker, K. Hanjalic, S. Kenjeres, M. Tummers, and H. J. Jonker, *Analysis and Modelling of Physical Transport Phenomena*. VSSD, 2008.

[8] M. Kadivar, D. Tormey, and G. McGranaghan, "A review on turbulent flow over rough surfaces: Fundamentals and theories," *International Journal of Thermofluids*, vol. 10, p. 100077, 5 2021.

[9] K. D. Ridder, "Bulk transfer relations for the roughness sublayer," *Boundary-Layer Meteorology*, vol. 134, pp. 257–267, 2010.

[10] U. Högström, "Review of some basic characteristics of the atmospheric surface layer," *Boundary-Layer Meteorology*, vol. 78, pp. 215–246, 1996.

[11] J. M. Donda, I. G. van Hooijdonk, A. F. Moene, H. J. Jonker, G. J. van Heijst, H. J. Clercx, and B. J. van de Wiel, "Collapse of turbulence in stably stratified channel flow: A transient phenomenon," *Quarterly Journal of the Royal Meteorological Society*, vol. 141, pp. 2137–2147, 7 2015.

[12] J. M. Donda, I. G. van Hooijdonk, A. F. Moene, G. J. van Heijst, H. J. Clercx, and B. J. van de Wiel, "The maximum sustainable heat flux in stably stratified channel flows," *Quarterly Journal of the Royal Meteorological Society*, vol. 142, pp. 781–792, 1 2016.

[13] J. G. Izett, B. Schilperoort, M. Coenders-Gerrits, P. Baas, F. C. Bosveld, and B. J. van de Wiel, "Missed fog?: On the potential of obtaining observations at increased resolution during shallow fog events," *Boundary-Layer Meteorology*, vol. 173, pp. 289–309, 11 2019.

[14] J. Izett, B. Schilperoort, M. Coenders, and B. J. H. B. van de Wiel, "High-Resolution DTS Temperature Measurements During Fog at Cabauw," 10 2018.

[15] B. Schilperoort, M. Coenders-Gerrits, C. sar Jim nez Rodr guez, C. V. D. Tol, B. V. D. Wiel, and H. Savenije, "Decoupling of a douglas fir canopy: A look into the subcanopy with continuous vertical temperature profiles," *Biogeosciences*, vol. 17, pp. 6423–6439, 12 2020.

[16] C. K. Thomas, A. M. Kennedy, J. S. Selker, A. Moretti, M. H. Schroth, A. R. Smoot, N. B. Tufillaro, and M. J. Zeeman, "High-resolution fibre-optic temperature sensing: A new tool to study the two-dimensional structure of atmospheric surface-layer flow," *Boundary-Layer Meteorology*, vol. 142, pp. 177–192, 2 2012.

[17] I. N. Harman and J. J. Finnigan, "A simple unified theory for flow in the canopy and roughness sublayer," *Boundary-Layer Meteorology*, vol. 123, pp. 339–363, 5 2007.

[18] B. B. Hicks and N. S. Eash, "On the effective surface temperature of a natural landscape: Infrared or not infrared," *Boundary-Layer Meteorology*, vol. 180, pp. 353–362, 8 2021.

[19] Z. Dong, S. Gao, and D. W. Fryrear, "Drag coefficients, roughness length and zero-plane displacement height as disturbed by artificial standing vegetation," *Journal of Arid Environments*, vol. 49, pp. 485–505, 2001. Raises the issue of differing characteristics as the displacement height, the roughness height and others as the density, length, roughness or other characteristics of the vegetation changes.

A. Numerical integration

The temperature profiles from the models in chapter 3 are found through numerical integration using the `scipy.integrate.quad` function in Python.

At first the models were integrated using a simplistic approximation where the surface underneath the function was approximated using

$$S(z_i) = \left.\frac{\partial T}{\partial z}\right|_{z_i} \cdot z_i.$$

Due to the low values of the gradient model as z becomes larger, this simplistic integration can deviate from the actual profile. This is therefore compared to the analytical integration and the `quad` quadratic method, see figure A.1 for the result.

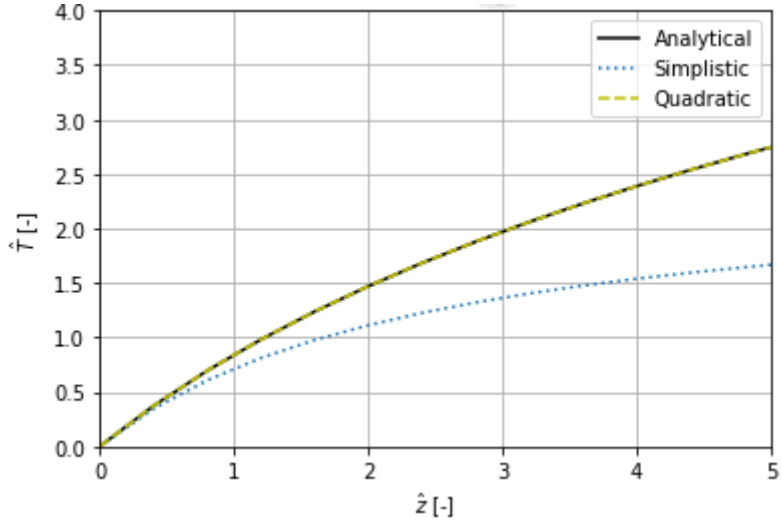

Figure A.1.: Comparison of the analytically integrated profile of the $z + b$ model (black full line) against the simplistic (blue dotted line) and quadratic integration (yellow striped line) methods. The quadratic profile overlaps the analytical solution and looks therefore as if it is a yellow line with black dots over it.

The figure shows that the quadratic numerical integration provides a close approximation with no visual difference to the analytical solution. The simplistic method was therefore replaced by the python function.

B. Selected data

Table B.1.: Overview of the selected data points or instances with the values associated with them. The column *Sun* indicates whether the Sun is up or down, *GH* is the grass height, *P* is the check if there is precipitation, T_{top} is the temperature at the top of the mast, T_{g} is the temperature at the lowest point of the mast, ΔT is the difference between these highest and lowest points, *Low* is the height of the lower boundary of the visually established log layer, *Upper* is the upper boundary, finally θ_* is the heat flux scale calculated for each instance.

Date	Time	Sun	GH	P	T_{top}	T_{g}	ΔT	Low	Upper	θ_*
d/m/y	h:m	u/d	cm	y/n	°C	°C	°	m	m	°
04/05	15:54	up	10	N	17.13	18.29	-1.16	4.091	6.818	-0.168
04/05	01:52	down	10	N	8.43	7.09	1.34	4.636	7.636	0.176
04/05	21:48	down	10	N	10.88	7.40	3.49	3.273	6.818	0.428
05/05	01:19	down	10	N	7.80	5.67	2.13	3.273	6.818	0.252
05/05	04:19	down	10	N	6.36	4.22	2.14	3.273	6.545	0.282
05/05	19:11	up	10	N	16.10	12.90	3.21	4.091	6.818	0.320
06/05	19:18	up	10	N	17.13	12.54	4.60	4.091	6.818	0.465
07/05	19:51	up	10	N	15.97	15.03	0.93	4.636	6.273	0.090
07/05	02:58	down	10	N	11.70	9.55	2.15	3.818	6.818	0.281
08/05	07:28	up	10	N	12.26	13.66	-1.40	3.273	5.455	-0.134
08/05	19:07	up	10	N	14.16	12.38	1.78	4.091	7.364	0.284
09/05	18:52	up	10	N	19.56	15.38	4.18	4.091	7.636	0.456
10/05	22:38	down	10	N	16.49	15.39	1.10	3.818	6.818	0.158
10/05	23:49	down	10	N	16.21	14.55	1.66	3.818	6.545	0.236
10/05	00:57	down	10	N	13.86	9.64	4.22	4.364	7.091	0.750
11/05	23:52	down	10	N	12.24	10.98	1.26	4.636	7.364	0.140
11/05	02:41	down	10	N	16.17	15.21	0.96	4.091	6.818	0.156
12/05	03:53	down	10	N	10.72	8.417	2.30	4.091	6.273	0.277
12/05	01:45	down	10	N	10.591	7.234	3.36	4.091	7.091	0.278
12/05	04:06	down	10	N	10.772	8.25	2.52	4.091	6.273	0.283
12/05	19:52	up	10	N	14.72	11.231	3.49	4.091	7.091	0.291
12/05	22:31	down	10	N	12.895	8.478	4.42	4.091	6.818	0.376
12/05	22:05	down	10	N	12.773	8.664	4.11	4.364	6.818	0.458
12/05	22:18	down	10	N	13.009	8.849	4.16	4.364	6.818	0.479
13/05	21:42	down	10	N	13.619	11.17	2.45	3.545	6.818	0.196
13/05	19:31	up	10	N	14.833	12.689	2.14	3.545	7.091	0.197
13/05	22:03	down	10	N	13.349	10.845	2.50	4.091	6.818	0.200
13/05	01:00	down	10	N	11.258	9.145	2.11	3.818	6.545	0.268
13/05	00:48	down	10	N	11.403	9.06	2.34	4.091	6.818	0.325
13/05	22:54	down	10	N	12.241	8.728	3.51	3.545	7.091	0.376
13/05	19:42	up	10	N	14.483	11.572	2.91	4.364	7.364	0.388

Table B.1.: (continued)

Date dd/mm	Time h:m	Sun u/d	GH cm	P y/n	T_{top} °C	T_g °C	ΔT °	Low m	Upper m	θ_* °
13/05	20:35	up	10	N	13.584	9.829	3.76	4.091	6.818	0.392
13/05	21:25	down	10	N	13.648	9.937	3.71	4.091	6.818	0.432
13/05	20:18	up	10	N	14.264	8.658	5.61	4.091	6.818	0.472
13/05	23:08	down	10	N	12.026	7.107	4.92	3.818	7.091	0.583
13/05	19:59	up	10	N	14.11	9.265	4.85	4.091	6.818	0.638

Colophon

This document was typeset using LaTeX, using the KOMA-Script class `scrbook`. The main font is Palatino.